International Journal of Solids and Structures 49 (2012) 865–880

Contents lists available at SciVerse ScienceDirect

International Journal of Solids and Structures

journal homepage: www.elsevier.com/locate/ijsolstr

A multi-scale enriched model for the analysis of masonry panels

Daniela Addessi [a,*], Elio Sacco [b]

[a] Dipartimento di Ingegneria Strutturale e Geotecnica, Università di Roma "Sapienza", Via Eudossiana 18, 00184 Roma, Italy
[b] Dipartimento di Meccanica, Strutture, Ambiente e Territorio, Università di Cassino, Via G. Di Biasio 43, 03043 Cassino, Italy

ARTICLE INFO

Article history:
Received 12 May 2011
Received in revised form 11 October 2011
Available online 29 December 2011

Keywords:
Multi-scale model
Masonry
Nonlinear homogenization
Damage–friction
Cosserat continuum

ABSTRACT

A multi-scale model for the structural analysis of the in-plane response of masonry panels, characterized by periodic arrangement of bricks and mortar, is presented. The model is based on the use of two scales: at the macroscopic level the Cosserat micropolar continuum is adopted, while at the microscopic scale the classical Cauchy medium is employed. A nonlinear constitutive law is introduced at the microscopic level, which includes damage, friction, crushing and unilateral contact effects for the mortar joints. The nonlinear homogenization is performed employing the Transformation Field Analysis (TFA) technique, properly extended to the macroscopic Cosserat continuum. A numerical procedure is developed and implemented in a Finite Element (FE) code in order to analyze some interesting structural problems. In particular, four numerical applications are presented: the first one analyzes the response of the masonry Representative Volume Element (RVE) subjected to a cyclic loading history; in the other three applications, a comparison between the numerically evaluated response and the micromechanical or experimental one is performed for some masonry panels.

1. Introduction

The masonry is a structural material obtained joining natural or artificial bricks by means of mortar layers. Thus, it is a heterogeneous material; for this reason, in the last 20 years, several researchers developed models based on the micromechanical analysis of the masonry, adopting homogenization techniques. In this framework, different constitutive masonry models have been proposed in the literature; they have been obtained according to the assumptions schematically reported below:

1. Arrangement of the masonry:
   (a) regular arrangement, i.e. masonry considered as a periodic composite material;
   (b) quasi-periodic or irregular texture of the masonry.
2. Model for the brick:
   (a) rigid;
   (b) deformable with linear response;
   (c) interface or continuum material characterized by nonlinear response.
3. Model for the mortar:
   (a) interface or continuum material characterized by linear response;
   (b) interface or continuum material characterized by nonlinear response;
4. Macroscopic model obtained by homogenization:
   (a) Cauchy continuum;
   (b) Cosserat or higher order continua.

Moreover, various homogenization techniques have been proposed and applied for masonry heterogeneous materials. Thus, selecting among the different possible mechanical assumptions and adopting different homogenization techniques, many masonry models and numerical procedures have been obtained.

From a review of the available literature, it can be noted that most of the references deal with the in-plane analysis of periodic masonry panels. In this framework, Cauchy models are recovered applying periodic homogenization techniques and considering the elastic behavior of both brick and mortar by Anthoine (1995) and Luciano and Sacco (1998). Nonlinear masonry models are proposed, for example, by Sacco (2009), assuming the elastic response of the brick and a coupled damage–friction model for the mortar. Furthermore, several models based on the nonlinear response of both the constituents of the masonry, brick and mortar, are presented in the literature. Among the others, Gambarotta and Lagomarsino (1997b) consider an equivalent stratified medium made up of mortar joints and brick units layers and adopt damage constitutive laws both for the bricks and the mortar joints. Massart et al. (2007) propose an enhanced multi-scale model using nonlocal implicit gradient isotropic damage models for both the constituents, describing the damage preferential orientations and employing at the macroscopic scale an embedded band model. Zucchini and Lourenco (2009) propose an improved micromechanical model for masonry

* Corresponding author. Tel.: +39 0644585298; fax: +39 064884852.
E-mail address: daniela.addessi@uniroma1.it (D. Addessi).

0020-7683/$ - see front matter © 2012 Elsevier Ltd. All rights reserved.
doi:10.1016/j.ijsolstr.2011.12.004

homogenization in the nonlinear domain, incorporating suitably chosen deformation mechanisms coupled with damage and plasticity models. Wei and Hao (2009) develop a continuum damage model for masonry accounting for the strain rate effect, using a homogenization theory implemented in a numerical algorithm.

In the framework of the Cosserat continuum models, Masiani et al. (1995) and Masiani and Trovalusci (1996) study the case of two-dimensional periodic rigid block assemblies joined by elastic mortar, deducing the macroscopic characterization of the equivalent medium by equating the virtual stress power of the coarse model with the virtual power of the internal actions of the discrete fine model. Salerno and de Felice (2009) investigate on the accuracy of various identification schemes for Cauchy and Cosserat continua, showing that in the case of non periodic deformation states micropolar continuum better reproduces the discrete solutions, due to its capability to take scale effects into account. Casolo (2006) considers isotropic linear elastic models both for the brick and the mortar and uses a computational approach to identify the homogenized elastic tensor of the equivalent Cosserat medium. Sab and Pradel (2009) present the development of homogenization procedures for Cosserat materials with periodic micro-structure, critically discussing about other existing homogenization procedures. Nonlinear response of the mortar joints is assumed by Addessi et al. (2010), using a cohesive-friction constitutive model. Moreover, nonlinear behavior for both brick and mortar is considered by De Bellis and Addessi (2011). An in-plane multi-level strategy is proposed by Brasile et al. (2007a,b) for the static and dynamical multi-scale analysis of masonry walls.

Most of the existing models for masonry concern periodic microstructures. Cecchi and Sab (2009) analyze non-periodic masonries, typical of historical buildings, by means of a perturbation approach, while Cavalagli et al. (2011) deal with the evaluation of the strength domain for non-periodic masonry using a random media micromechanical approach.

Also the out-of-plane analysis of masonry panels is a very important and interesting issue. In fact, recent earthquakes show that the out-of-plane failure of masonry walls is responsible of the loss of human life. Mercatoris and Massart (2011) presents a multi-scale framework for the failure of periodic quasi-brittle thin planar shells, using a shear-enhanced element with the Reissner-Mindlin description and employing it for the failure of out-of-plane loaded masonry walls.

With the aim of satisfactorily describing the structural behavior of masonry panels, reproducing accurately both the global and local response, a reliable masonry model should account for the nonlinear response of the constituents and the deformability of the bricks. In particular, because of the cohesive (quasi-brittle) response of the masonry material constituents, softening effects arise in the stress–strain relationship, which can induce localization of deformations and damage in structural analyses, when the classical Cauchy continuum model is adopted. In order to overcome such drawbacks, nonlocal approaches or higher-order continuum models can be adopted. Moreover, spurious localization can be mitigated also introducing special tricks within the FE method. To this end, one simple and widely adopted approach to overcome the localization problem is the fracture energy regularization (Bazant and Planas, 1998). More sophisticated methods consist in the enrichment of the kinematic description in the FE, considering for instance the presence of strong discontinuities in the displacement field (Linder and Armero, 2007). On the other hand, a homogenization method leading to a Cauchy continuum is unable to predict size effects in the mechanical behavior of heterogeneous materials. Then, the adoption of a generalized continuum gives a natural way to obtain an explicit dependence of the effective properties of composites or multiphase materials on the absolute size of the constituents with a continuum model and to account for size effects.

The Cosserat model can be considered as an effective approach both from a mechanical point of view, mainly when the size of the microstructure is relevant, and for computational reasons, since it allows to naturally regularize the problem in the case of predominant shearing damaging mechanisms in the masonry panels.

In this paper a multi-scale approach for the analysis of the in-plane masonry response is presented, adopting a Cosserat model at the macro-level and a classical Cauchy medium at the micro-structural level. The choice of using two different continuum models is based on the following considerations. At the macro-scale, as remarked above, the adoption of the micropolar Cosserat model allows to account for the internal length of the material and to mitigate or overcome localization problems. From a mechanical point of view, the Cosserat rotation field can describe the rotation of the bricks composing the masonry texture, mainly when the mortar joints are damaged. However, it can be emphasized that the setting of the Cosserat elastic moduli is not straightforward. Thus, the homogenization procedure based on the micromechanical analysis of the RVE allows to rationally derive the components of the elastic Cosserat matrix. On the other hand, at the micro-scale level the classical Cauchy model can be considered absolutely satisfactory. Various examples of coupling two different continuum models can be found in literature. Forest and Sab (1998) use a Cosserat continuum at the macro-level and a Cauchy medium at the micro-level, applying the homogenization procedure to a multi-layer composite material. Kouznetsova et al. (2002) present a gradient-enhanced computational procedure that extends the classical computational homogenization technique to a full-gradient geometrically nonlinear approach. They adopt a higher-order continuum at the macroscopic level, while the microstructural constituents are modeled as a classical Cauchy continuum. This may have advantages over the modeling of the microstructure by a generalized continuum, since, for nonlinear material behavior, the formulation of constitutive equations and experimental procedures for material parameter identification are sufficiently developed and verified in the framework of classical continuum models. A second-order computational homogenization of heterogeneous materials is proposed by Bacigalupo and Gambarotta (2011). The computational procedure is derived assuming an appropriate representation of the micro-displacement field as the superposition of a local macroscopic displacement field and an unknown micro-fluctuation field accounting for the effects of the heterogeneities.

In the present work regular arrangements of bricks and mortar are considered, assuming a linear elastic behavior for the brick and a damage-plastic constitutive law, which accounts for the internal friction effect, for the mortar joints. The proposed constitutive model takes into account also the crushing plasticity mechanisms. Furthermore, a degrading exponential law is adopted for the friction parameter in order to reproduce the experimental results. A homogenization technique is developed to identify the equivalent Cosserat macroscopic continuum model. In particular, in order to account for the nonlinear behavior of the mortar joints, the Transformation Field Analysis (TFA) technique, originally presented by Dvorak (1992) and recently proposed by Addessi et al. (2010) for the micromechanical analysis of the masonry RVE, is herein adopted. A multi-scale computational strategy is developed and implemented in the Finite Element (FE) code FEAP (Taylor, 2011). Numerical applications are finally presented to investigate on the ability of the proposed model to reproduce the mechanical response of masonry panels and to assess the effectiveness and robustness of the developed numerical procedure. To this end, comparisons with micromechanical and experimental tests are performed, investigating both on the global response and on the local mechanisms. In Section 2 the two boundary value problems (BVP) formulated at the macro- and micro-scale are introduced; in Section 3, the description of the TFA-based nonlinear homogeni-

zation procedure is given; in Section 4, the numerical procedure and the developed solution algorithm is described; lastly, in Section 5 some numerical examples are reported. Finally, comments and remarks on the developed model and the implemented computational procedure are given.

2. Multi-scale model for periodic masonry

A two-scale model for the analysis of 2D masonry structures is introduced, based on the adoption of the Cosserat continuum at the structural macro-level and the classical Cauchy medium at the micro-level. The proposed multi-scale approach is based on the complete separation of the two scales and a homogenization procedure is employed to rationally derive the constitutive relationship at each macroscopic integration point. To this end, the equilibrium equations are satisfied with zero body force at the micro-scale, together with the compatibility and constitutive laws of the single constituents. At the structural scale, equilibrium and compatibility are satisfied, while the constitutive relations are derived by means of the homogenization technique from the micro-scale. This multi-scale approach, which can be considered the most classical and popular micro–macro procedure, is defined as 'uncoupled multi-scale mathematical model' by Fish and Shek (2000). As remarked by Fish and Shek (2000), it can be applied with satisfactory approximation for large scale problems, i.e. when the size of the structure is much greater than the size of the microstructure, otherwise coupled models have to be used.

As widely shown in literature, the enriched micropolar Cosserat model at the macro-level allows to account for the microstructural interaction effects, related to the size and shape of the constituents, on the structural response. On the other hand, most of the damage-plastic constitutive models proposed in literature for masonry constituents are formulated and identified in the framework of the classical Cauchy continuum, thus suggesting the adoption of the Cauchy model at the micro-level.

In the spirit of the multi-scale procedure, two BVPs are formulated at the macro- and micro-level, respectively, together with a properly conceived kinematic map connecting the two levels and getting information across them. In the following, the equations governing the two BVPs and the adopted nonlinear homogenization procedure are illustrated. Small strain and displacement assumptions hold.

2.1. Macro-level BVP

At the macro-level, where the Cosserat continuum model is employed, the displacement vector $\mathbf{U} = \{U_1 \; U_2 \; \Phi\}^T$ contains three independent kinematic fields, representing the translations U_1 and U_2 and the rotation Φ, respectively, at each point $\mathbf{X} = (X_1, X_2)^T$ of the body volume Ω. The compatibility equations, relating the deformation components to the displacement fields, are introduced in compact form as:

$$\mathbf{E} = \mathbf{D}\mathbf{U} \quad \text{in } \Omega \tag{1}$$

whose expanded form is:

$$\begin{Bmatrix} E_1 \\ E_2 \\ \Gamma_{12} \\ \Theta \\ K_1 \\ K_2 \end{Bmatrix} = \begin{bmatrix} \frac{\partial}{\partial X_1} & 0 & 0 \\ 0 & \frac{\partial}{\partial X_2} & 0 \\ \frac{\partial}{\partial X_2} & \frac{\partial}{\partial X_1} & 0 \\ -\frac{\partial}{\partial X_2} & \frac{\partial}{\partial X_1} & -2 \\ 0 & 0 & \frac{\partial}{\partial X_1} \\ 0 & 0 & \frac{\partial}{\partial X_2} \end{bmatrix} \begin{Bmatrix} U_1 \\ U_2 \\ \Phi \end{Bmatrix} \tag{2}$$

where $\mathbf{E}$ is the strain vector and $\mathbf{D}$ the compatibility operator. The first three components of $\mathbf{E}$ are the in-plane Cauchy extensional and symmetric shear strains, $\Theta = E_{12} - E_{21} = 2(W - \Phi)$ is the rotational deformation, representing two times the difference between the rigid rotation W and the Cosserat rotation field Φ, being:

$$W = \frac{1}{2}\left(\frac{\partial U_2}{\partial X_1} - \frac{\partial U_1}{\partial X_2}\right) \tag{3}$$

and K_1 and K_2 are the curvatures.

Accordingly, the stress vector $\mathbf{\Sigma}$ is expressed as:

$$\mathbf{\Sigma} = \{\, \Sigma_1 \quad \Sigma_2 \quad \Sigma_{12} \quad Z \quad M_1 \quad M_2 \,\}^T \tag{4}$$

where Σ_1 and Σ_2 are the normal stresses, Σ_{12} is the symmetric shear stress, Z is the stress component associated to the rotational deformation Θ and M_1 and M_2 are the couples. The equilibrium equations result as:

$$\mathbf{D}^T\mathbf{\Sigma} + \mathbf{B} = \mathbf{0} \quad \text{in } \Omega \tag{5}$$

where the vector $\mathbf{B}$ is formed by two components of body forces, namely B_1 and B_2, and one component of body couple C.

The displacement and traction boundary conditions are defined as follows:

$$\mathbf{U} = \bar{\mathbf{U}} \quad \text{on } \partial\Omega_U, \qquad \mathbf{N}\mathbf{\Sigma} = \mathbf{T} \quad \text{on } \partial\Omega_T \tag{6}$$

where $\bar{\mathbf{U}}$ is the displacement vector prescribed on the boundary portion $\partial\Omega_U$, $\mathbf{N}$ is the matrix containing the unit vectors normal to the traction boundary contour $\partial\Omega_T$ and $\mathbf{T}$ is the vector of the external tractions.

A homogenization procedure is applied in order to derive the constitutive response in each macroscopic material point by means of the analysis of the corresponding RVE. In particular, for each RVE a BVP is solved, whose formulation is described in the following section, and the stress field calculated at the micro-level is homogenized to obtain the macroscopic stress components by applying the generalized Hill–Mandel principle. Thus, the macroscopic elastic constitutive tensor $\mathbf{C}$, obtained by applying the homogenization technique on a RVE characterized by an orthotropic texture of the masonry, is expressed in the following form (Trovalusci and Masiani, 1999):

$$\mathbf{C} = \begin{bmatrix} C_{11} & C_{12} & 0 & 0 & 0 & 0 \\ C_{21} & C_{22} & 0 & 0 & 0 & 0 \\ 0 & 0 & C_{33} & C_{34} & 0 & 0 \\ 0 & 0 & C_{43} & C_{44} & 0 & 0 \\ 0 & 0 & 0 & 0 & D_{11} & 0 \\ 0 & 0 & 0 & 0 & 0 & D_{22} \end{bmatrix} \tag{7}$$

where the first 3×3 sub-matrix can be recognized as the standard in-plane elastic constitutive operator for the Cauchy continuum with $C_{12} = C_{21}$, $C_{34} = C_{43}$ and C_{44} governing the skew-symmetric shear behavior, influenced by the shape of the RVE; D_{11} and D_{22} govern the flexural behavior affected by the absolute size of the RVE. It has to be noted that, when the damaging process starts and evolves, the RVE response may become anisotropic and, as a consequence, the tangent constitutive tensor $\mathbf{C}$ is not characterized by the orthotropic structure reported in (7) anymore. Nevertheless, the adopted homogenization procedure, described in the following, makes use of the elastic orthotropic constitutive tensor (7).

2.2. Micro-level BVP

In the following the equations governing compatibility, equilibrium and constitutive behavior of the masonry RVE are introduced in the 2*D* framework. The analysis is limited to the case of periodic masonry made of regular textures of bricks and mortar joints.

The displacement vector $\mathbf{u} = \{u_1, u_2\}^T$ at each point $\mathbf{x} = \{x_1, x_2\}^T$ of the RVE occupying the volume ω at a given loading step is intro-

duced in a representation form as the superposition of a prescribed field $\bar{\mathbf{u}}$, defined as function the macroscopic deformation $\mathbf{E}$, and an unknown periodic fluctuation $\tilde{\mathbf{u}}$, satisfying proper periodicity conditions on the RVE boundary (Suquet, 1987; Luciano and Sacco, 1998), namely:

$$\mathbf{u} = \bar{\mathbf{u}}(\mathbf{x}) + \tilde{\mathbf{u}}(\mathbf{x}) \quad \text{in } \omega \tag{8}$$

with:

$$\tilde{\mathbf{u}} \quad \text{periodic on } \partial\omega \tag{9}$$

The compatibility equations are expressed in compact form as:

$$\boldsymbol{\varepsilon} = \mathbf{d}\mathbf{u} \quad \text{in } \omega \tag{10}$$

where $\mathbf{d}$ is the compatibility operator and $\boldsymbol{\varepsilon}$ the strain vector, which accordingly to Eq. (8) may be expressed as:

$$\boldsymbol{\varepsilon} = \bar{\boldsymbol{\varepsilon}}(\mathbf{x}) + \tilde{\boldsymbol{\varepsilon}}(\mathbf{x}) \tag{11}$$

being $\bar{\boldsymbol{\varepsilon}}$ and $\tilde{\boldsymbol{\varepsilon}}$ the strain fields compatible with $\bar{\mathbf{u}}$ and $\tilde{\mathbf{u}}$, respectively. The expanded form of Eq. (10) is:

$$\begin{Bmatrix} \varepsilon_1 \\ \varepsilon_2 \\ \gamma_{12} \end{Bmatrix} = \begin{bmatrix} \frac{\partial}{\partial x_1} & 0 \\ 0 & \frac{\partial}{\partial x_2} \\ \frac{\partial}{\partial x_2} & \frac{\partial}{\partial x_1} \end{bmatrix} \begin{Bmatrix} u_1 \\ u_2 \end{Bmatrix} \tag{12}$$

Considering zero body forces acting on the RVE, the equilibrium equations result as:

$$\mathbf{d}^T\boldsymbol{\sigma} = \mathbf{0} \quad \text{in } \omega \tag{13}$$

where the vector $\boldsymbol{\sigma}$, representing a self-equilibrated stress field, collects the stress components as:

$$\boldsymbol{\sigma} = \{\, \sigma_1 \quad \sigma_2 \quad \tau_{12} \,\}^T \tag{14}$$

and satisfies the following boundary conditions:

$$\mathbf{n}\boldsymbol{\sigma} \quad \text{anti-periodic on } \partial\omega \tag{15}$$

where $\mathbf{n}$ denotes the matrix of the outward unit vectors normal to $\partial\omega$.

Some authors in literature, as for example Pegon and Anthoine (1997) and Massart et al. (2005), proposed to adopt the generalized plane state conditions in order to model the in-plane behavior of the RVE masonry, mainly when compressive failure mechanisms occur. Herein, a simplified generalized plane state is considered. In fact, let t be the masonry thickness, and A^B and A^M the areas of the mid-surface of the brick and mortar, respectively, as illustrated in Fig. 1. When the masonry is subjected to the vertical compressive stress σ_2, together with the vertical contraction, a dilatation ε_3 is expected for the masonry. Note that, if the wall is large enough along the x_1-direction and it is properly restrained to the soil, the strain ε_1 can be considered as negligible. Assuming the same values for the vertical normal stress σ_2 and for the dilatation ε_3 in the brick and the mortar, with the in-plane strain $\varepsilon_1 = 0$, and considering both the brick and the mortar as elastic isotropic materials, the following constitutive equations can be written:

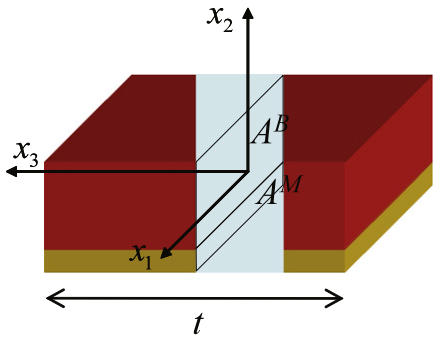

Fig. 1. Brick and mortar arrangement along the masonry thickness.

$$\sigma_2 = 2\mu^B\varepsilon_2^B + \lambda^B(\varepsilon_2^B + \varepsilon_3) \tag{16}$$

$$\sigma_2 = 2\mu^M\varepsilon_2^M + \lambda^M(\varepsilon_2^M + \varepsilon_3) \tag{17}$$

$$\sigma_3^B = 2\mu^B\varepsilon_3 + \lambda^B(\varepsilon_2^B + \varepsilon_3) \tag{18}$$

$$\sigma_3^M = 2\mu^M\varepsilon_3 + \lambda^M(\varepsilon_2^M + \varepsilon_3) \tag{19}$$

with μ^B, λ^B, μ^M and λ^M, the Lamé constants for the brick and mortar. The average transversal stress is computed and enforced to be equal to zero:

$$\bar{\sigma}_3 = \frac{A^B}{A^B + A^M}\sigma_3^B + \frac{A^M}{A^B + A^M}\sigma_3^M = 0 \tag{20}$$

Eqs. (16)–(20) represent a set of five equations in the five unknowns ε_2^B, ε_2^M, ε_3, σ_3^B and σ_3^M. Once the system is solved, the effective Poisson ratios of the brick and mortar can be evaluated as:

$$\bar{\nu}^B = -\frac{\varepsilon_3}{\varepsilon_2^B}, \quad \bar{\nu}^M = -\frac{\varepsilon_3}{\varepsilon_2^M} \tag{21}$$

Hence, developing the 2D plane stress analysis by assuming the Poisson ratios evaluated by formulas (21), the transversal deformation of the masonry is allowed with negligible average transversal stress, when the RVE is mainly loaded in vertical compression, as it occurs in the masonry panels.

At the micro-level the nonlinear constitutive behavior of the masonry constituents is known and formulated in detail. As for the brick, the linear elastic stress–strain relationship is adopted:

$$\boldsymbol{\sigma}^B = \mathbf{C}^B\boldsymbol{\varepsilon} \tag{22}$$

where $\mathbf{C}^B$ is the elastic matrix and $\boldsymbol{\sigma}^B = \{\sigma_1^B, \sigma_2^B, \tau_{12}^B\}^T$ is the stress vector in the brick.

A realistic modeling of the masonry material requires the use of a nonlinear constitutive law at least for the mortar component, considering the damage and the friction effects. A formulation of the mortar joint model, which considers the effects of the cohesion, damage and friction is proposed by Gambarotta and Lagomarsino (1997a). They introduce two internal variables representing the frictional sliding and the mortar joint damage, adopting a phenomenological evolution law for the damage variable, based on the R-curve approach.

A coupled damage-plastic constitutive law for the mortar material is herein adopted. The plastic-damage friction constitutive model proposed in the present work is derived on the basis of a simple but consistent micromechanical analysis of the damaging mechanism of the mortar joint, based on an idea originally presented by Ragueneau et al. (2000) and for interfaces by Alfano and Sacco (2006), properly modified to model the mortar behavior by Sacco (2009) and recently used by Addessi et al. (2010).

Herein, the model is enriched introducing an exponential law which describes the evolution of the friction parameter. Furthermore, in order to take into account the crushing mechanism of the masonry a limit compressive stress is considered. Indeed, the crushing of the masonry panel is generally due to the failure of the bricks; in order to work with a simpler model, leaving a linear elastic stress–strain relationship for the bricks, the compressive crushing is introduced in the mortar constitutive law.

A local coordinate system is introduced in the typical mortar joint, with T and N denoting directions parallel and orthogonal to the mortar joint, respectively.

An additive decomposition of the stress vector $\boldsymbol{\sigma}^M$ at a typical point of the mortar is assumed as follows:

$$\boldsymbol{\sigma}^M = (1 - D)\boldsymbol{\sigma}^u + D\boldsymbol{\sigma}^d \tag{23}$$

where D is the scalar damage parameter, measuring the ratio between the damaged part of the representative mortar area and the total representative area. The two stress vectors $\boldsymbol{\sigma}^u$ and $\boldsymbol{\sigma}^d$ are related to the strain vector in the mortar, $\boldsymbol{\varepsilon}$, by the constitutive equations:

$$\boldsymbol{\sigma}^u = \mathbf{C}^M(\boldsymbol{\varepsilon} - \mathbf{p}), \quad \boldsymbol{\sigma}^d = \mathbf{C}^M(\boldsymbol{\varepsilon} - \boldsymbol{\varepsilon}^p - \mathbf{p}) \tag{24}$$

where

$$\mathbf{C}^M = \begin{bmatrix} C^M_{TT} & C^M_{NT} & 0 \\ C^M_{NT} & C^M_{NN} & 0 \\ 0 & 0 & G^M \end{bmatrix} \tag{25}$$

represents the elasticity matrix of the mortar, $\boldsymbol{\varepsilon}^p$ is the vector of the strain accounting for the possible unilateral opening effect and for the friction sliding, while $\mathbf{p}$ is the plastic strain due to the crushing.

Taking into account the constitutive Eqs. (24), Eq. (23) becomes:

$$\boldsymbol{\sigma}^M = \mathbf{C}^M(\boldsymbol{\varepsilon} - \boldsymbol{\pi}) \tag{26}$$

where $\boldsymbol{\pi}$ is the vector collecting all the inelastic strains, conveniently written in the form:

$$\boldsymbol{\pi} = \begin{Bmatrix} \pi_T \\ \pi_N \\ \pi_{NT} \end{Bmatrix} = \begin{Bmatrix} 0 \\ p_N \\ 0 \end{Bmatrix} + D \begin{Bmatrix} h(\varepsilon_N - p_N)\varepsilon_T \\ h(\varepsilon_N - p_N)(\varepsilon_N - p_N) \\ \gamma^p_{NT} \end{Bmatrix} \tag{27}$$

accounting for the crushing, p_N, the damage, D, the unilateral contact by means of the component $h(\varepsilon_N - p_N)(\varepsilon_N - p_N)$ and the slip by means of the component γ^p_{NT}; $h(\varepsilon_N - p_N)$ is the Heaviside function, which assumes the following values: $h(\varepsilon_N - p_N) = 0$ if $(\varepsilon_N - p_N) \leqslant 0$ and $h(\varepsilon_N - p_N) = 1$ if $(\varepsilon_N - p_N) > 0$. Because of the simplified form of the inelastic strain (27), the constitutive law (24) is able to provide zero normal stress in transversal direction, $\sigma^d_N = 0$, as well as in longitudinal direction, $\sigma^d_T = 0$, when opening of the mortar joint occurs.

The crushing and the friction effects are modeled as classical plasticity problems. The evolution law of the crushing inelastic strain component p_N is stated as:

$$\dot{p}_N = -\dot{\lambda}_p \tag{28}$$

and it is ruled by the Kuhn–Tucker conditions, being λ_p the inelastic multiplier:

$$\dot{\lambda}_p \geqslant 0, \quad \psi(\boldsymbol{\sigma}) \leqslant 0, \quad \dot{\lambda}_p \psi(\boldsymbol{\sigma}) = 0 \tag{29}$$

The yield function is assumed as:

$$\psi(\boldsymbol{\sigma}) = -(\sigma_N + \sigma_y + \alpha\xi) \tag{30}$$

where σ_y is the compressive yield threshold, $\alpha \leqslant 0$ is the softening parameter and ξ is the total plastic strain evaluated as:

$$\xi = \int_0^t |\dot{p}_N| d\tau \tag{31}$$

As concerning the friction mechanism, the evolution of the inelastic slip strain component γ^p_{NT} is governed by the Coulomb yield function:

$$\varphi(\boldsymbol{\sigma}^d) = \mu(\zeta)\sigma^d_N + |\tau^d_{NT}| \tag{32}$$

where μ is the friction parameter evolving according to the following exponential law:

$$\mu(\zeta) = (\mu_f - \mu_i)(1 - e^{-\delta\zeta}) + \mu_i \tag{33}$$

being μ_i and μ_f the initial and final friction values, respectively, δ the exponential rate parameter and ζ the total plastic slip strain, defined as:

$$\zeta = \int_0^t |\dot{\gamma}^p_{NT}| d\tau \tag{34}$$

A non-associated flow rule is considered as:

$$\dot{\gamma}^p_{NT} = \dot{\lambda} \frac{\tau^d_{NT}}{|\tau^d_{NT}|} \tag{35}$$

with the following loading–unloading Kuhn–Tucker conditions:

$$\dot{\lambda} \geqslant 0 \quad \varphi(\boldsymbol{\sigma}^d) \leqslant 0, \quad \dot{\lambda}\ \varphi(\boldsymbol{\sigma}^d) = 0 \tag{36}$$

where λ is the inelastic multiplier.

A model which accounts for the coupling of mode I and mode II of fracture is considered for the evolution of the damage parameter D. The two quantities η_N and η_{NT}, which depend on the first cracking strains $\varepsilon_{N,0}$ and $\gamma_{NT,0}$, on the peak values of the stresses $\sigma_{N,0}$ and $\tau_{NT,0}$ and on the fracture energies G_{cI} and G_{cII}, respectively, are introduced in the form:

$$\eta_N = \frac{\varepsilon_{N,0}\sigma_{N,0}}{2G_{cI}}, \quad \eta_{NT} = \frac{\gamma_{NT,0}\tau_{NT,0}}{2G_{cII}} \tag{37}$$

The equivalent strain measures Y_N and Y_{NT} are defined as:

$$Y_N = (\langle \varepsilon_N - p_N \rangle)^2, \quad Y_{NT} = (\gamma_{NT})^2 \tag{38}$$

where the bracket operator $\langle \cdot \rangle$ gives the positive part of the quantity $\cdot$. Then, the strain ratios are determined as:

$$\eta = \frac{1}{\alpha^2}(Y_N\eta_N + Y_{NT}\eta_{NT}), \quad \beta = \sqrt{\frac{Y_N}{\varepsilon^2_{N,0}} + \frac{Y_{NT}}{\gamma^2_{NT,0}}}, \quad \alpha = \sqrt{Y_N + Y_{NT}} \tag{39}$$

Finally, the damage is evaluated according to the following law:

$$D = \max_{\text{history}}\{\min\{1, \bar{D}\}\} \quad \text{with } \bar{D} = \frac{\beta - 1}{(1 - \eta)\beta} \tag{40}$$

3. Homogenization technique

The constitutive response in each macroscopic point of the equivalent Cosserat continuum is derived by adopting the compatible nonlinear homogenization procedure presented in Addessi et al. (2010), based on the TFA technique. In the following, the main steps of such methodology are illustrated.

First of all, taking into consideration that the definition of the RVE in the framework of the Cosserat homogenized medium affects the mechanical characterization of the equivalent Cosserat continuum deduced by the homogenization procedure and influences the overall structural response, herein the RVE is chosen as the simplest repetitive cell. The selected RVE is characterized by

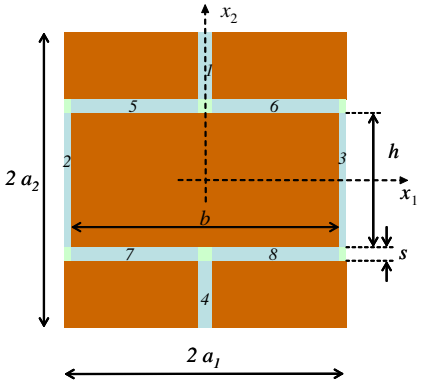

Fig. 2. Selected RVE: running bond texture.

rectangular shape with dimensions $2a_1$ and $2a_2$, parallel to the coordinate axes x_1 and x_2, as shown in Fig. 2. The RVE accounts for all the geometrical and constitutive properties of the masonry components; in Fig. 2, the mortar thickness is denoted by s and the brick sizes by b and h.

3.1. Kinematic map

The first step of the compatible homogenization procedure is to establish a kinematic map linking the macro- and micro-level. Herein, following the methodology proposed by Forest and Sab (1998), third order polynomial expansions are assumed for the assigned part of the microscopic displacement $\bar{\mathbf{u}}(\mathbf{x})$, which allows to take into account all the macroscopic Cosserat deformation components. In the case of a rectangular cell, the following form of the assigned displacement $\bar{\mathbf{u}}$ is adopted in compact notation:

$$\bar{\mathbf{u}} = \mathbf{A}(\mathbf{x})\mathbf{E} \tag{41}$$

where

$$\mathbf{A} = \begin{bmatrix} x_1 & 0 & \frac{1}{2}x_2 & -\alpha(x_2^3 - 3\rho^2 x_1^2 x_2) & -x_1x_2 & -\frac{1}{2}x_2^2 \\ 0 & x_2 & \frac{1}{2}x_1 & -\rho^2\alpha(\rho^2 x_1^3 - 3x_1x_2^2) & \frac{1}{2}x_1^2 & x_1x_2 \end{bmatrix} \tag{42}$$

with

$$\alpha = \frac{5}{4}\frac{a_1^2 + a_2^2}{a_1^4}, \quad \rho = \frac{a_2}{a_1} \tag{43}$$

In order to activate the Cauchy deformation modes independently from the Cosserat ones, in Eq. (41) the fourth component of the Cosserat strain vector $\mathbf{E}$ is redefined as:

$$\widehat{\Theta} = \Theta + \frac{1}{2}\frac{\rho^2 - 1}{\rho^2 + 1}\Gamma_{12} \tag{44}$$

The stress variable conjugated to $\widehat{\Theta}$ is denoted with $\widehat{Z}$.

The strain vector at the micro-level (Eq. (11)) can now be expressed as:

$$\boldsymbol{\varepsilon} = \mathbf{B}(\mathbf{x})\mathbf{E} + \tilde{\boldsymbol{\varepsilon}}(\mathbf{x}) \tag{45}$$

where $\tilde{\boldsymbol{\varepsilon}}(\mathbf{x})$ is the periodic strain, satisfying null average condition in ω, and:

$$\mathbf{B} = \begin{bmatrix} 1 & 0 & 0 & 6\alpha\rho^2 x_1 x_2 & -x_2 & 0 \\ 0 & 1 & 0 & 6\alpha\rho^2 x_1 x_2 & 0 & x_1 \\ 0 & 0 & 1 & 3\alpha(\rho^2 - 1)(x_2^2 - \rho^2 x_1^2) & 0 & 0 \end{bmatrix} \tag{46}$$

The in-plane periodicity and continuity conditions (9) lead to the following boundary conditions:

$$\begin{aligned} &\tilde{\mathbf{u}}(a_1, x_2) = \tilde{\mathbf{u}}(-a_1, x_2) \quad \forall x_2 \in [-a_2, a_2] \\ &\tilde{\mathbf{u}}(x_1, a_2) = \tilde{\mathbf{u}}(x_1, -a_2) \quad \forall x_1 \in [-a_1, a_1] \end{aligned} \tag{47}$$

3.2. Nonlinear homogenization

The masonry RVE is subjected to the macroscopic Cosserat strain $\mathbf{E}$ applied to the whole RVE and to the inelastic strain $\boldsymbol{\pi}^i$, with $i = 1,\ldots,m$, applied to each of the m mortar joints.

The micromechanical BVPs on the RVE, subjected to the prescribed value of the six components of $\mathbf{E}$ and to the three components of the inelastic strains $\boldsymbol{\pi}^i$ in the m mortar joints, have to be solved. The micromechanical strain field, resulting after solving the BVP on the RVE subjected to $\mathbf{E}$, can be written in the following representation form:

$$\mathbf{e} = \mathbf{R}_e(\mathbf{x})\mathbf{E} \tag{48}$$

where the localization matrix $\mathbf{R}_e(\mathbf{x})$ is introduced. Consequently, the average strain in the brick and in each mortar joint M^i results as:

$$\bar{\mathbf{e}}^B = \bar{\mathbf{R}}_e^B\mathbf{E}, \quad \bar{\mathbf{e}}^{M^i} = \bar{\mathbf{R}}_e^{M^i}\mathbf{E} \tag{49}$$

where $\bar{\mathbf{R}}_e^B$ and $\bar{\mathbf{R}}_e^{M^i}$ denote the average localization matrices in the brick volume and in the mortar joint volume, respectively.

The homogenized Cosserat stress in the whole RVE volume ω is obtained by applying the generalized Hill–Mandel principle, resulting:

$$\boldsymbol{\Sigma}_e = \mathbf{C}\mathbf{E} \tag{50}$$

where the overall elastic constitutive matrix is defined as:

$$\mathbf{C} = \frac{1}{\omega}\left[\int_B \mathbf{R}_e^T\mathbf{C}^B\mathbf{e}\,d\omega + \sum_{j=1}^{m}\int_{M^j}\mathbf{R}_e^T\mathbf{C}^{M^j}\mathbf{e}\,d\omega\right] \tag{51}$$

Moreover, the average stress in the mortar joint M^i may be evaluated as $\bar{\boldsymbol{\sigma}}_e^{M^i} = \mathbf{C}^M\bar{\mathbf{e}}^{M^i} = \mathbf{C}^M\bar{\mathbf{R}}_e^{M^i}\mathbf{E}$, as well as in the brick $\bar{\boldsymbol{\sigma}}_e^B = \mathbf{C}^B\bar{\mathbf{e}}^B = \mathbf{C}^B\bar{\mathbf{R}}_e^B\mathbf{E}$.

Similarly, after solving the micromechanical problem of the RVE subjected to an inelastic strain $\boldsymbol{\pi}^i$ prescribed in the mortar joint M^i, the resulting local strain field is expressed in the form:

$$\mathbf{p}^i = \mathbf{R}_{\pi^i}(\mathbf{x})\boldsymbol{\pi}^i \tag{52}$$

being $\mathbf{R}_{\pi^i}(\mathbf{x})$ the associated localization matrix. Note that the local strain field $\mathbf{p}^i$ is characterized by null average. The elastic strain in the typical mortar joint M^j results as:

$$\boldsymbol{\eta}^{i,M^j} = \mathbf{p}^{i,M^j} - \delta_{ij}\boldsymbol{\pi}^i = \left(\mathbf{R}_{\pi^i}^{M^j} - \delta_{ij}\mathbf{I}\right)\boldsymbol{\pi}^i \quad \text{(no sum)} \tag{53}$$

where $\mathbf{p}^{i,M^j}$ and $\mathbf{R}_{\pi^i}^{M^j}$ are the restriction to the mortar M^j of the fields $\mathbf{p}^i$ and $\mathbf{R}_{\pi^i}$, respectively. The elastic strain in the brick coincides with the total strain:

$$\boldsymbol{\eta}^{i,B} = \mathbf{p}^{i,B} = \mathbf{R}_{\pi^i}^B\boldsymbol{\pi}^i \tag{54}$$

with evident meaning of the symbols. The corresponding overall Cosserat stress can be obtained again by applying the generalized Hill–Mandel principle in the form:

$$\begin{aligned} \boldsymbol{\Sigma}_{\pi^i} &= \frac{1}{\omega}\left[\int_B \left(\mathbf{R}_{\pi^i}^B\right)^T\mathbf{C}^B\boldsymbol{\eta}^{i,B}\,d\omega + \sum_{j=1}^{m}\int_{M^j}\left(\mathbf{R}_{\pi^i}^{M^j}\right)^T\mathbf{C}^{M^j}\boldsymbol{\eta}^{i,M^j}\,d\omega\right] \\ &= \frac{1}{\omega}\left[\int_B \left(\mathbf{R}_{\pi^i}^B\right)^T\mathbf{C}^B\mathbf{R}_{\pi^i}^B\,d\omega + \sum_{j=1}^{m}\int_{M^j}\left(\mathbf{R}_{\pi^i}^{M^j}\right)^T\mathbf{C}^{M^j}\left(\mathbf{R}_{\pi^i}^{M^j} - \delta_{ij}\mathbf{I}\right)d\omega\right]\boldsymbol{\pi}^i \end{aligned} \tag{55}$$

Aiming to express the macroscopic constitutive law in the form:

$$\boldsymbol{\Sigma} = \mathbf{C}(\mathbf{E} - \mathbf{P}) = \mathbf{C}\mathbf{E}_e \tag{56}$$

where $\mathbf{E}_e = \mathbf{E} - \mathbf{P}$ is the overall elastic strain, the RVE is subjected to the overall elastic strain $\mathbf{E}_e$ and to the inelastic strains $\boldsymbol{\pi}^i$, $i = 1,2,\ldots,m$, and superposition of the effects is heuristically performed. In fact, it is possible to compute the overall stress as:

$$\boldsymbol{\Sigma} = \boldsymbol{\Sigma}_e + \sum_{i=1}^{m}\boldsymbol{\Sigma}_{\pi^i} = \mathbf{C}\mathbf{E} + \sum_{i=1}^{m}\boldsymbol{\Sigma}_{\pi^i} \tag{57}$$

so that the inelastic strain $\mathbf{P}$ can be defined as:

$$\mathbf{P} = -\mathbf{C}^{-1}\sum_{i=1}^{m}\boldsymbol{\Sigma}_{\pi^i} \tag{58}$$

Moreover, the total average strain in the m mortar joints is determined as:

$$\bar{\boldsymbol{\varepsilon}}^{M^j} = \bar{\mathbf{R}}_e^{M^j}\mathbf{E} + \bar{\mathbf{R}}_{\pi^i}^{M^j}\boldsymbol{\pi}^i \tag{59}$$

and the average stresses in the m mortar joints and in the brick are given by:

$$\begin{aligned}\bar{\boldsymbol{\sigma}}^{M^j} &= \mathbf{C}^M\left(\bar{\mathbf{e}}^{M^j} + \bar{\boldsymbol{\eta}}^{1,M^j} + \cdots + \bar{\boldsymbol{\eta}}^{m,M^j}\right) = \mathbf{C}^M\left(\bar{\boldsymbol{\varepsilon}}^{M^j} - \boldsymbol{\pi}^j\right)\\ \bar{\boldsymbol{\sigma}}^{B} &= \mathbf{C}^B\left(\bar{\mathbf{e}}^{B} + \bar{\boldsymbol{\eta}}^{1,B} + \cdots + \bar{\boldsymbol{\eta}}^{m,B}\right) = \mathbf{C}^B\bar{\boldsymbol{\varepsilon}}^{B}\end{aligned} \tag{60}$$

Herein, it is assumed that:

- the inelastic strain is constant in each mortar joint;
- the nonlinear behavior of the RVE depends on the average stresses and strains evaluated in each of the m mortar joints.

4. Computational procedure

The FE method is used to solve the BVPs at the macro- and micro-level. At the macro-level a 2*D* 4-node quadrilateral FE is implemented to discretize the Cosserat medium, with three degrees of freedom at each node, two translational and one rotational. Instead, a standard Cauchy 4-node quadrilateral FE is adopted to model the RVE level with two translational degrees of freedom at each node. A step-by-step solution technique based on the classical backward-Euler algorithm (Simo and Hughes, 1998) is adopted for the integration of the governing equations, using a constant time step $\Delta t = t_{n+1} - t_n$. The nonlinear problem in each time step is solved by means of the Newton–Raphson technique.

The proposed nonlinear homogenization procedure initially requires the evaluation of the overall constitutive matrix $\mathbf{C}$ and of the localization matrices $\bar{\mathbf{R}}_e^{M^j}$ and $\bar{\mathbf{R}}_{\pi}^{M^j}$. They are computed by solving $6 + 3m$ FE linear elastic micromechanical problems at the RVE level.

Table 1
Damage-plastic solution procedure in the mortar joint M^j

Iteration '$k+1$'
Crushing evaluation
– Prediction phase
– Trial yield function
$\psi^{k+1,tr} = -(\sigma_N^{k+1,tr} + \sigma_y + \alpha\xi^{k+1,tr})$
– Check plasticity
If $\psi^{k+1,tr} < 0 \Rightarrow \Delta\lambda_p^{k+1} = 0$, else
– Correction phase
$\Delta\lambda_p^{k+1} = \frac{\psi^{k+1,tr}}{C_{TT}^M - \alpha}$ with
$\Delta\lambda_p^{k+1} \geqslant 0 \quad \psi^{k+1} \leqslant 0, \quad \Delta\lambda_p^{k+1}\ \psi^{k+1} = 0$
$\Delta p_N^{k+1} = -\Delta\lambda_p^{k+1}$
$\xi^{k+1} = \xi_n + \lvert\Delta p_N^{k+1}\rvert$
Damage evaluation
– Equivalent strain measures
$Y_N^k = \left(< \varepsilon_N^k - p_N^{k+1} >\right)^2, \quad Y_{NT}^k = (\gamma_{NT}^k)^2$(Eq. (38))
– Strain ratios
η^k, β^k (Eq. (39))
– Damage
D^{k+1} (Eq. (40))
Unilateral effect evaluation
If $\left(\varepsilon_N^k - p_N^{k+1}\right) \leqslant 0$ then $h^{k+1} = 0$ else $h^{k+1} = 1$
If $D^{k+1} > 0$
Friction plasticity evaluation
– Prediction phase
$\boldsymbol{\pi}^{k+1,tr} = \boldsymbol{\pi}_n^i \ (i = 1,\ldots,m)$
$\zeta^{k+1,tr} = \zeta_n$
– Trial yield function
$\varphi^{k+1,tr} = \mu(\zeta^{k+1,tr})\sigma_N^{d\,k+1,tr} + \left\lvert\tau_{NT}^{d\,k+1,tr}\right\rvert$
– Check plasticity
If $\varphi^{k+1,tr} < 0 \Rightarrow \Delta\gamma_{NT}^{p,k+1} = 0$, else
– Correction phase
$\Delta\lambda^{k+1} = \frac{1}{G^M}\varphi^{k+1,tr}$ with
$\Delta\lambda^{k+1} \geqslant 0\ \varphi^{k+1} \leqslant 0,\ \Delta\lambda^{k+1}\varphi^{k+1} = 0$
$\Delta\gamma_{NT}^{p,k+1} = \Delta\lambda\frac{\tau_{NT}^{d\,k+1,tr}}{\left\lvert\tau_{NT}^{d\,k+1,tr}\right\rvert}$
$\zeta^{k+1} = \zeta_n + \lvert\Delta\gamma_{NT}^{p,k+1}\rvert$
μ^{k+1} (Eq. (33))

After that, the multi-scale solution procedure starts and goes on as described in the following, denoting with the subscript 'n' the variables evaluated at the previous time step t_n and using no subscript to indicate the corresponding current quantities, i.e. computed at the step t_{n+1}. Moreover, Δ denotes the increment of the variable in the time step Δt.

In the spirit of the displacement-based FE method, at the current Newton–Raphson iteration the increment of the nodal displacements at the macro-level discretization is evaluated. Then, the macroscopic Cosserat strain vector increment $\Delta\mathbf{E}$ is computed at each Gauss integration point and the strain vector $\mathbf{E}$ is updated. At this stage, the damage and plasticity evolution problem on the RVE subjected to the macroscopic Cosserat total strain $\mathbf{E}$ is solved, by adopting a return-mapping algorithm in order to evaluate the overall Cosserat stress $\boldsymbol{\Sigma}$. To this end, the strain $\mathbf{E}$ and the inelastic strains $\boldsymbol{\pi}^j$ ($j = 1,2,\ldots,m$), related to the crushing, damage and to the unilateral contact-friction effects occurring in the mortar joints, have to be calculated.

It is worthwhile noting that, as it is clear from Eq. (59), the average strain $\bar{\boldsymbol{\varepsilon}}^{M^j}$ in the mortar joint M^j depends on the overall strain $\mathbf{E}$ and on all the m inelastic strains $\boldsymbol{\pi}^i$ ($i = 1,2,\ldots,m$). Consequently, the nonlinear evolution problems in the m mortar joints result all coupled, giving rise to a complex nonlinear problem. Then, by exploiting the splitting procedure, the iterative procedure described below is employed, solving a set of m uncoupled evolutionary problems, one for each mortar joint, considering as frozen the crushing, damage and friction evolution into the others $m - 1$.

At the previous iteration k, the macroscopic Cosserat elastic strain $\mathbf{E}_e$ is evaluated on the basis of the total strain $\mathbf{E}$ and of the macroscopic strain $\mathbf{P}$ associated to all the inelastic strains $\boldsymbol{\pi}^i$ in

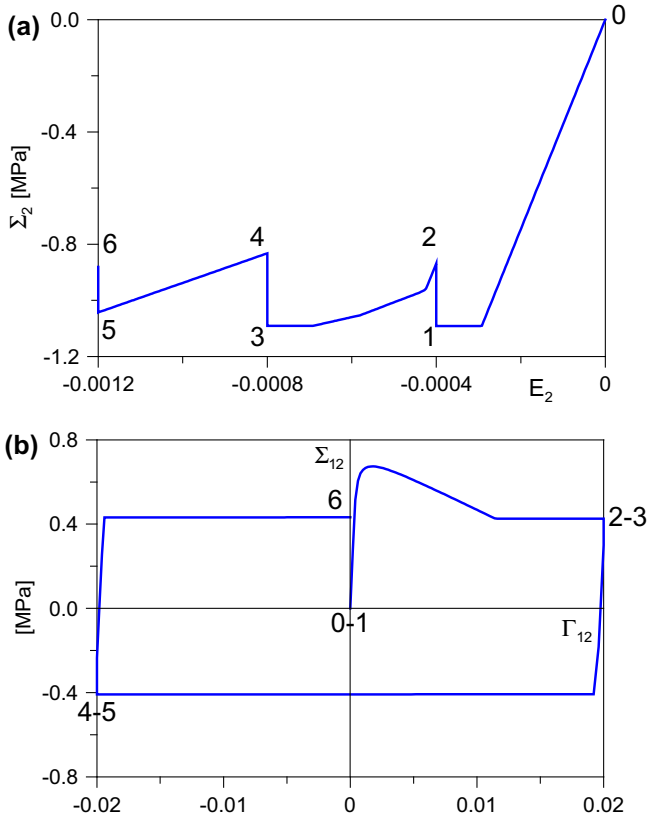

Fig. 3. RVE response: (a) normal stress Σ_2 versus normal strain E_2 and (b) shear stress Σ_{12} versus shear strain Γ_{12}.

the mortar joints. Then, the total and elastic average strains in the mortar joints, $\bar{\boldsymbol{\varepsilon}}^{M^j}$ and $\bar{\boldsymbol{\eta}}^{i,M^j}$, are computed.

At the current iteration and for all the mortar joints M^j, the crushing plastic strains are evaluated by means of a prediction-correction technique on the basis of the $\bar{\boldsymbol{\varepsilon}}^{M^j}$ evaluated at the previous iteration. Then, after updating the elastic normal strain in each mortar on the basis of the current crushing plastic strains, the damage associated variables Y_N and Y_{NT} together with the strain ratios η and β are computed and the damage variable is updated. Then, the unilateral contact problem is solved, by evaluating the Heaviside function $h(\varepsilon_N - p_N)$. Finally, if damage is active in the mortar joint M^j, the friction problem is solved adopting a prediction–correction technique. A trial prediction of the inelastic strains $\boldsymbol{\pi}^i$ is computed by assuming them equal to the ones evaluated at the previous time step t_n. The normal and trial shear stresses are then evaluated, on the basis of which the trial yield function φ is calculated. The correction phase is performed if $\varphi > 0$. Once the damage, the unilateral contact and the friction problems are solved in all the mortar joint M^j, the values of the inelastic strain vectors $\boldsymbol{\pi}^j$ are updated, then the new values of the total average strains $\bar{\boldsymbol{\varepsilon}}^{M^j}$ are determined. Thus, a further iteration is performed where compressive plasticity, damage, unilateral contact and friction problems have to be solved again in all the mortar joints, until a convergence test is satisfied. The scheme of the described solution algorithm is reported in Table 1, where the apex 'M^j' is omitted for easier notation.

Writing Eq. (59) in residual form, the residual strain can be evaluated in each mortar joint as:

$$\boldsymbol{\rho}^{M^j,k+1} = \bar{\mathbf{R}}_e^{M^j}\mathbf{E} + \sum_{i=1}^{m} \bar{\mathbf{R}}_{\pi^i}^{M^j}\boldsymbol{\pi}^{i,k+1} - \bar{\boldsymbol{\varepsilon}}^{M^j,k+1} \tag{61}$$

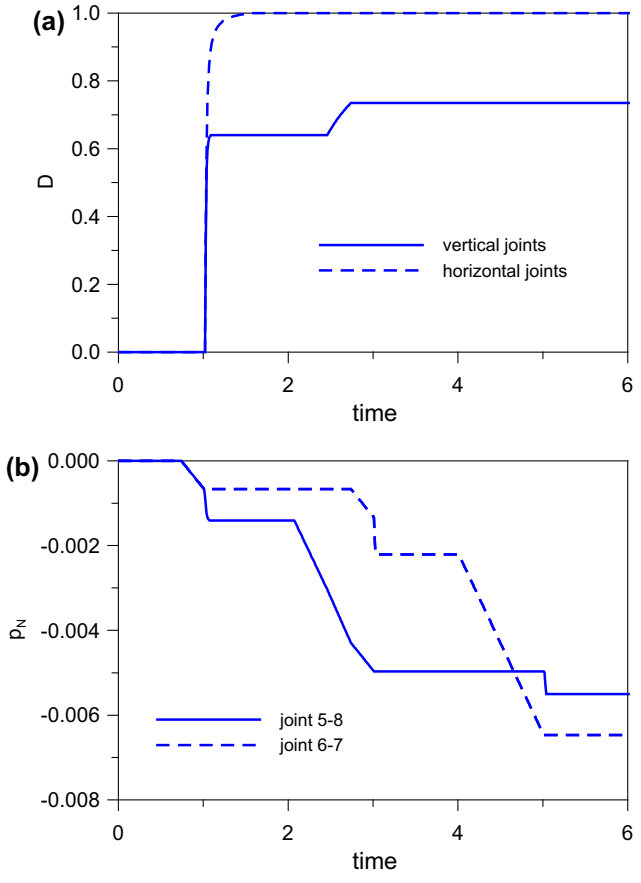

Fig. 4. RVE response: (a) damage evolution in mortar joints and (b) crushing plasticity evolution in the horizontal mortar joints.

The norm of the residual vectors, representing the residual error at the end of the $k+1$th iteration in each mortar joint, is computed as $\rho^{k+1} = \sum_{i=1}^{m} \|\boldsymbol{\rho}^{M^i,k+1}\|$. If the error is lower than a given tolerance the iterative procedure is stopped. At this point, the macroscopic stress vector $\boldsymbol{\Sigma}$ can be updated, passed back to the macroscopic Gauss point and used to evaluate the element residual vector at the $k+1$th iteration of the Newton–Raphson global solution procedure. The multi-scale model described above is implemented in the FE numerical code FEAP (Taylor, 2011).

5. Numerical results

In this section, the presented multi-scale procedure is employed to analyze the micromechanical response of the RVE and the structural response of masonry panels. In particular, the results obtained with the multi-scale model are compared both with micromechanical results and with experimental ones. The studied cases are characterized by a running bond texture. The number of mortar joints considered in the analysis of the RVE is set equal to 8, as shown in Fig. 2, where also the number associated to each joint is reported. As for the geometrical and mechanical parameters, the values adopted in the following structural analyses are derived from the data given in the micromechanical and experimental tests.

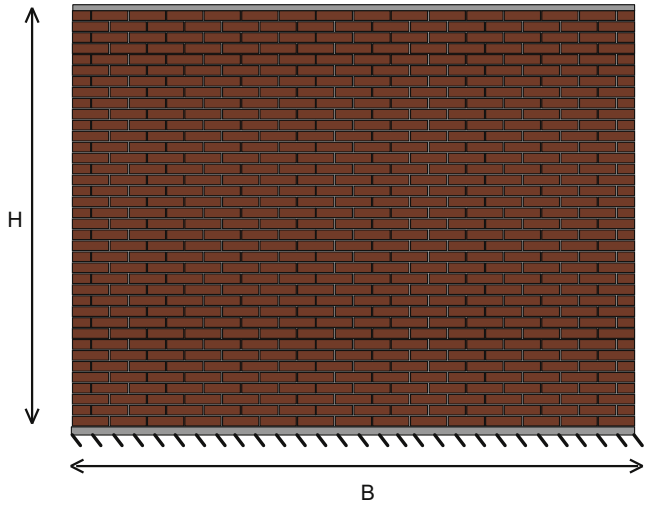

Fig. 5. Masonry panel under horizontal displacement: geometry and boundary conditions.

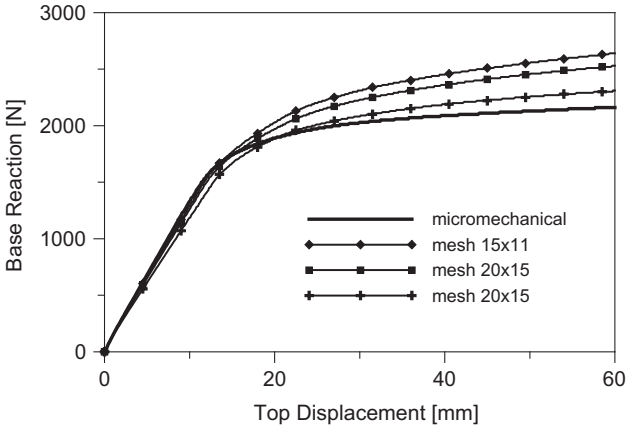

Fig. 6. Masonry panel under horizontal displacement: global response curve.

5.1. RVE micromechanical response

The RVE mechanical response is firstly analyzed assuming the following parameters: size of the brick $b = 210$ mm, $h = 52$ mm; thickness of the mortar joints $s = 10$ mm. The material mechanical parameters are:

	E (MPa)	ν	$\varepsilon_{N,0}$	$\gamma_{NT,0}$	G_{cI} (MPa)	G_{cII} (MPa)	μ	σ_y (MPa)	α (MPa)
Brick	16,700	0.15							
Mortar	798	0.11	0.0003	0.001	0.00179	0.0126	0.5	1.2	0

where a constant value is assumed for the friction parameter. As remarked in Sections 2.2 and 3.1, the homogenization is performed following the displacement-driven approach for the micromechanical problem, enforcing periodic boundary conditions. A detailed discussion of the homogenization approaches and of the possible boundary conditions can be found in Suquet (1987). Moreover, numerical tests showing as the displacement and the stress formulation of the homogenization problem, with periodic boundary conditions, converge from the above and from the below, respectively, to the exact solution of the RVE mechanical response are reported in Luciano and Sacco (1998). For the RVE herein considered, the components of the homogenized elastic tensor (7), obtained considering periodic boundary conditions, results:

$$C_{11} = 8513.20, \quad C_{12} = C_{21} = 336.83, \quad C_{22} = 3733.20$$
$$C_{33} = 1390.78, \quad C_{34} = C_{43} = 321.92, \quad C_{44} = 3803.43$$
$$C_{55} = 14739300, \quad C_{66} = 18350600$$

The obtained values represent the best estimation of the homogenized elastic tensor components. In fact, in the framework of the displacement formulation, the uniform displacement and the uniform traction boundary conditions lead to over-estimation and under-estimation of the elastic properties, respectively, as shown by a number of authors (van der Sluis et al., 2000; Terada et al., 2000). For instance, in the case of the analyzed RVE, the uniform displacement boundary conditions lead to the following over-estimation of the elastic tensor components:

$$C_{11} = 9978.42, \quad C_{12} = C_{21} = 457.99, \quad C_{22} = 4184.39$$
$$C_{33} = 1950.80, \quad C_{34} = C_{43} = -692.35, \quad C_{44} = 6944.50$$
$$C_{55} = 15781455, \quad C_{66} = 19400510$$

A cyclic loading history is assigned to the RVE combining compressive and symmetric shear strains, while all the other strain components are zero:

t	0	1	2	3	4	5	6
$E_2(E-4)$	0	4	4	8	8	12	12
$\Gamma_{12}(E-4)$	0	0	200	200	−200	−200	0

During the loading history the following stages can be distinguished in the RVE response:

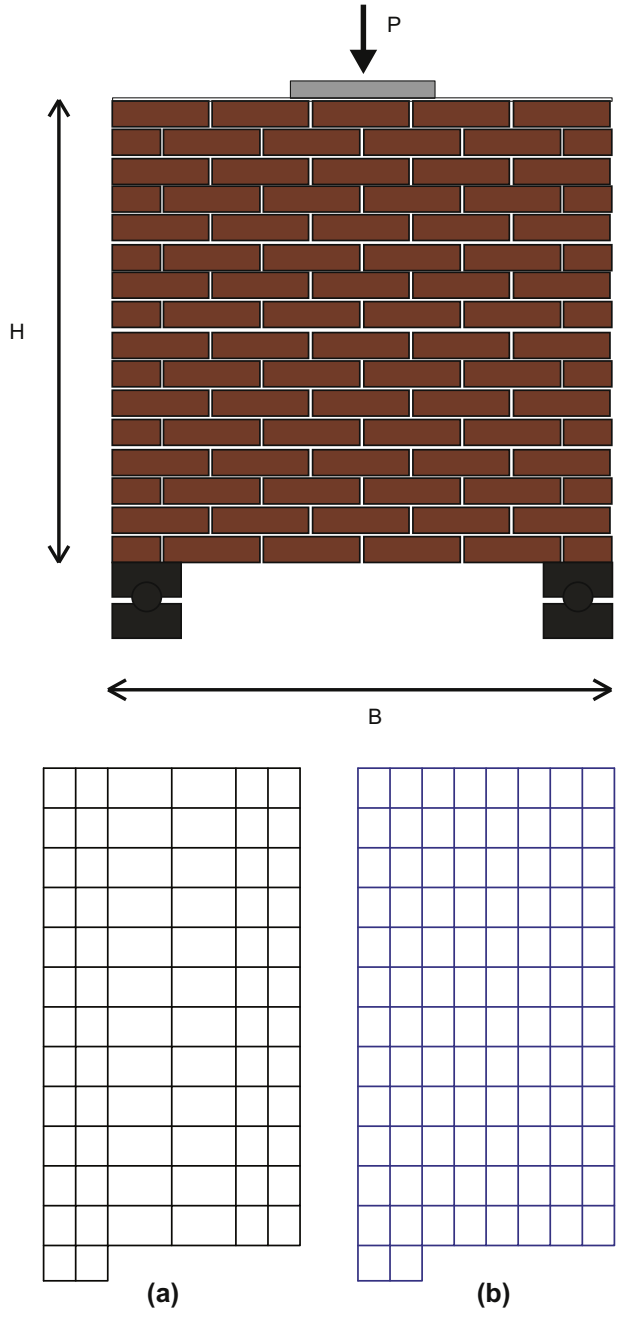

Fig. 7. Masonry panel under vertical load: geometry and boundary conditions.

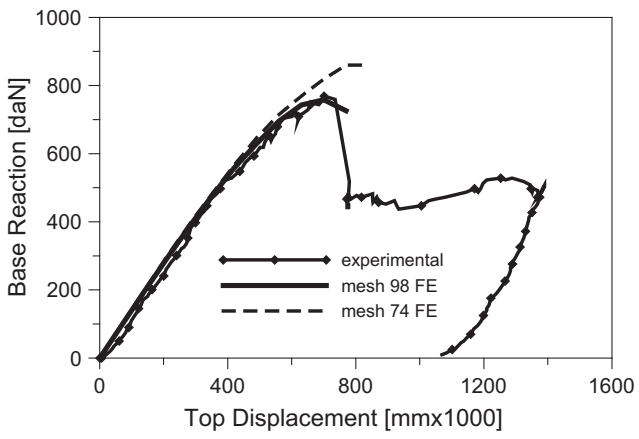

Fig. 8. Masonry panel under vertical load: global response curve.

0–1 Initially a compressive loading phase (Fig. 3(a)) is performed, where the crushing yield limit is reached and the crushing plasticity flow is activated into the horizontal joints (Fig. 4(b)), leading to the same plastic strain in the horizontal joints 5, 6, 7 and 8.

1–2 The symmetric shear strain is applied, taking the compressive strain constant. The $\Sigma_{12} - \Gamma_{12}$ curve in Fig. 3(b) shows a softening behavior followed by the friction plasticity response. The damage grows quickly both in the horizontal joints, which reach the completely damaged state, and in the vertical joints, which are partially damaged, as shown in Fig. 4(a). Note that during this phase the overall compressive normal stress decreases, due to the effect of the applied shear strain, which reduces the compression in the joints 6 and 7, while the joints 5 and 8 remain subjected to the limit compressive stress, increasing suddenly their crushing plastic strain.

2–3 Then, the compression strain is further increased, taking the symmetric shear strain constant, and the damage grows in the vertical joints. Again the crushing yield limit is reached and the plastic variable p_N grows in the horizontal joints (Fig. 4(b)), suddenly in the joints 5 and 8 and after in the joints 6 and 7, which have been unloaded during the phase 1–2.

3–4 A reverse symmetric shear strain is applied now; initially an elastic unloading phase is experienced, followed by the friction plasticity mechanism, as evident in Fig. 3(b). The damage remains constant in the vertical joints, while the

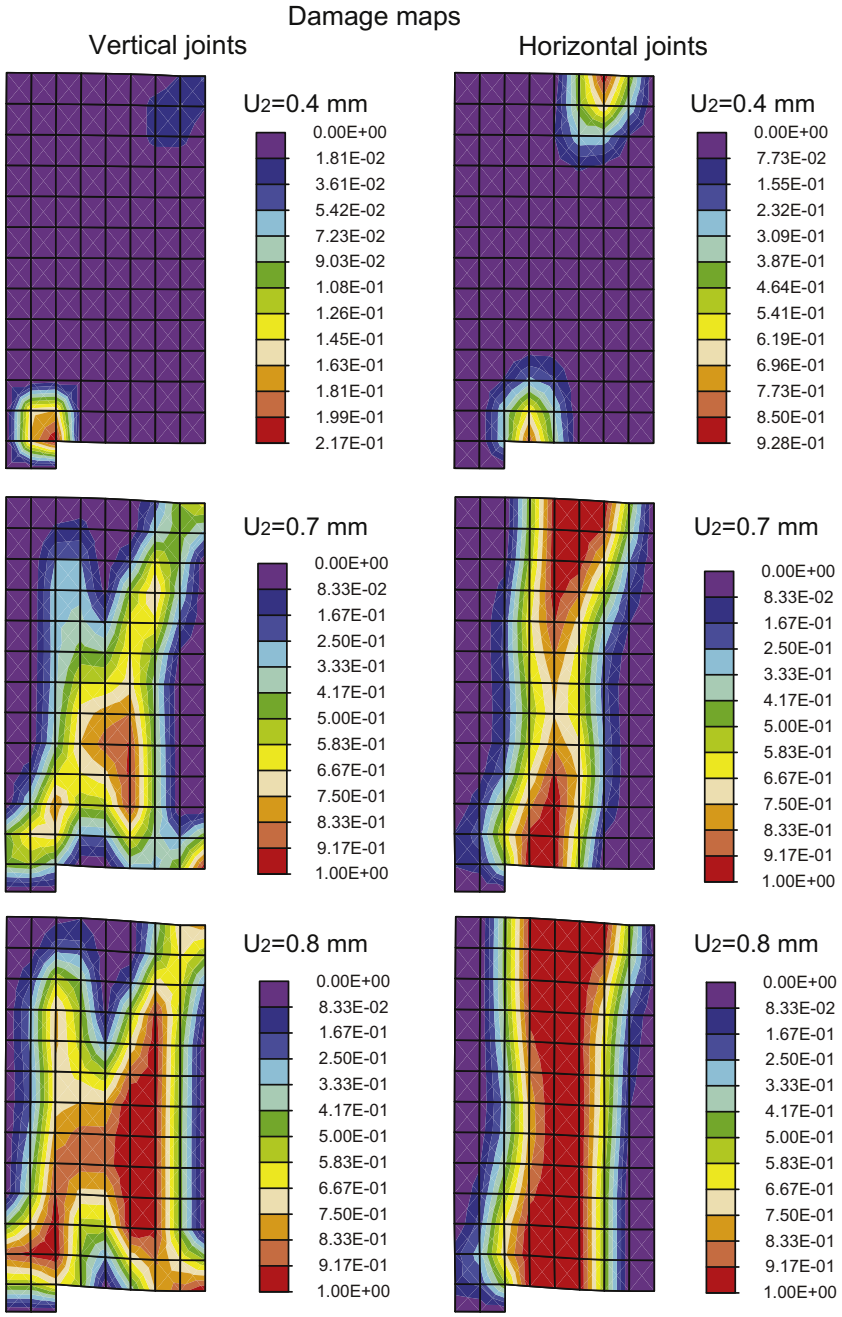

Fig. 9. Masonry panel under vertical load: damage distributions in vertical (left column) and horizontal joints (right column) evaluated at different values of the applied vertical displacement.

plastic variable p_N grows rapidly in the joints 6 and 7, remaining constant in the joints 5 and 8, which result unloaded during this phase.

4–5 The compression strain reaches its final value (Fig. 3(b)). The damage does not evolve anymore, while crushing plasticity increases in the joints 6 and 7.

5–6 A final unloaded shear phase follows, until the overall shear stress Σ_{12} becomes zero. Now both the damage and the plasticity do not evolve. The overall compressive stress Σ_2 decreases due to the unloading of the joints 6 and 7.

5.2. Micromechanical vs multi-scale analysis of a masonry panel

The structural response of the masonry panel shown in Fig. 5 is firstly analyzed. The sizes of the panel are: width $B = 3290$ mm, eight $H = 2356$ mm, thickness $T = 100$ mm. Both the top and the bottom sides are completely restrained. The panel is subjected initially to a vertical compressive displacement v applied at the top side equal to 10 mm. Subsequently, a horizontal displacement u monotonically increasing until the value of 60 mm is applied to the top side nodes. The geometrical parameters of bricks and mortar are the following: size of the brick $b = 210$ mm, $h = 52$ mm; thickness of the mortar joints $s = 10$ mm. The material mechanical parameters are:

	E (MPa)	ν	$\varepsilon_{N,0}$	$\gamma_{NT,0}$	G_{cI} (MPa)	G_{cII} (MPa)	μ
Brick	16,700	0.15					
Mortar	798	0.11	0.0003	0.001	0.00179	0.0126	0.45

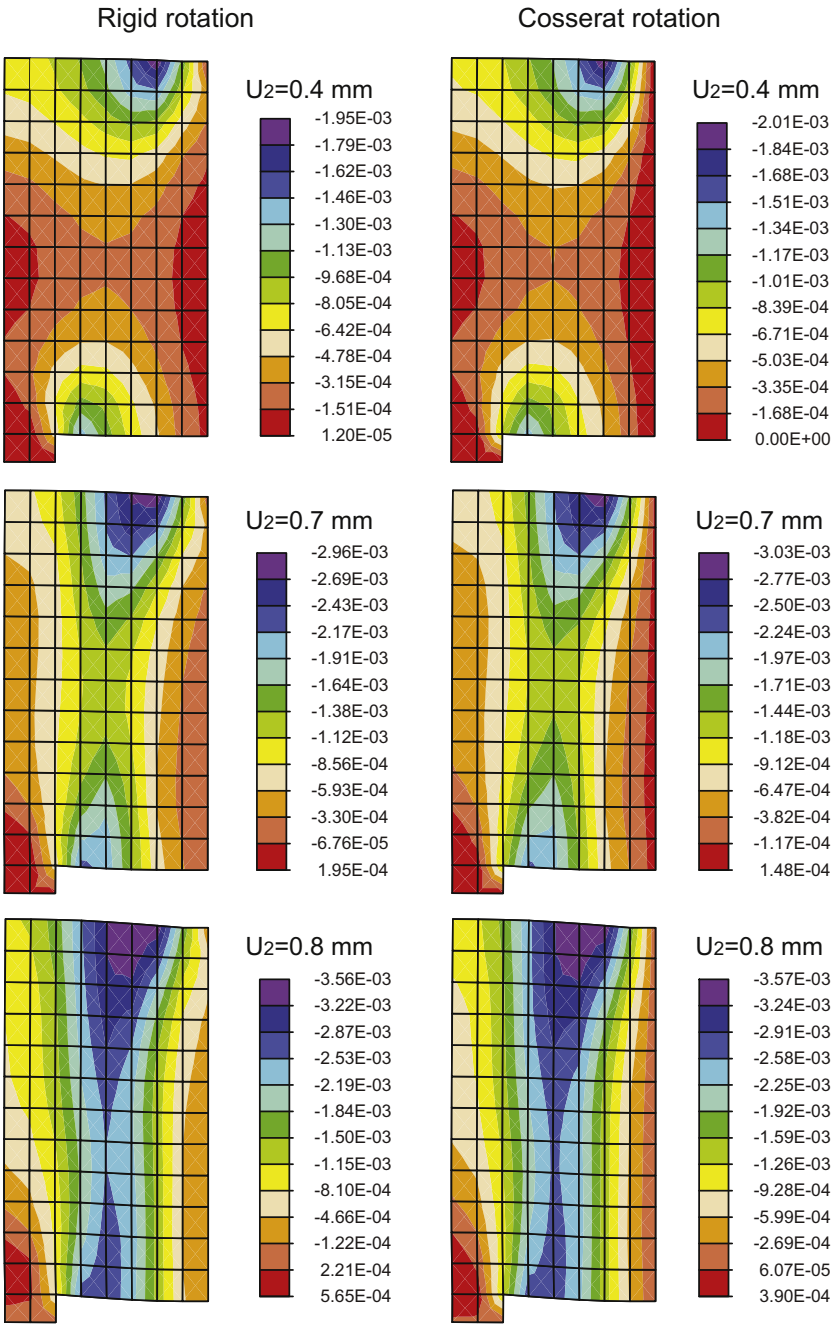

Fig. 10. Masonry panel under vertical load: rigid rotation (left column) and Cosserat rotation (right column) evaluated at different values of the applied vertical displacement.

where E and ν are Young's and Poisson moduli, respectively, and a constant friction parameter is considered, while the crushing plasticity is neglected. The numerical response evaluated by adopting the presented multi-scale model is compared with the results obtained by performing a micromechanical analysis, where bricks and mortar are discretized separately by 4-node quadrilateral Cauchy FEs assuming the constitutive laws presented in Section 2.2. As concerning the multi-scale analysis, two different meshes are adopted with 15×11 and 20×15 FEs, respectively, while 39,710 FEs are used for the micromechanical discretization with 152,760 degrees of freedom. In Fig. 6 the global response curves are reported showing the base horizontal reaction versus the top applied horizontal displacement. The solid line refers to the micromechanical result, while the lines with symbols refer to the multi-scale analyses performed with the 15×11 (line with diamonds) and 20×15 (line with squares) meshes and restraining completely the degrees of

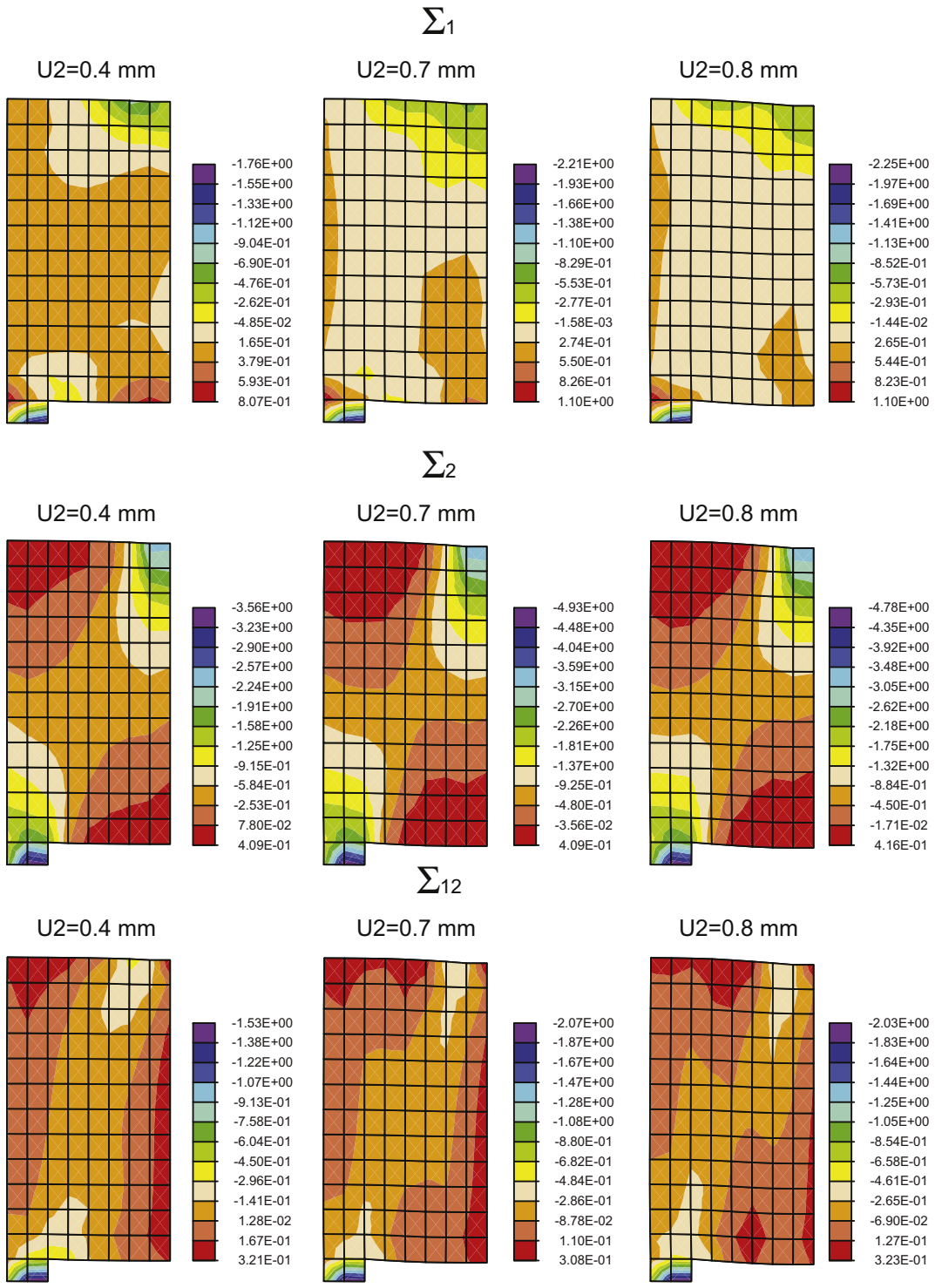

Fig. 11. Masonry panel under vertical load: macroscopic stresses Σ_1 (first row), Σ_2 (second row) and Σ_{12} (third row) evaluated at different values of the applied vertical displacement.

freedom at the top and bottom sides; the line with crosses refers to the 20×15 mesh where only the two translational degrees of freedom are restrained at the horizontal sides. Note that a very good agreement is obtained in the initial elastic branch, while the curves obtained with the multi-scale model depart a little from the micromechanical results in the nonlinear range, due to the capability of the micromechanical model of describing more accurately the nonlinear damaging and plasticity mechanisms. Furthermore, it appears that when the rotation degree of freedom is not restrained at the horizontal sides (line with crosses) the multi-scale model fits better the nonlinear micromechanical response.

5.3. Masonry panel under vertical load

The masonry panel acting as a deep beam shown in Fig. 7 was analyzed experimentally by Grande et al. (2008). The dimensions of the panel are: width $B = 290$ mm, eight $H = 270$ mm, thickness $T = 30$ mm. In the experimental tests the panel was restrained at

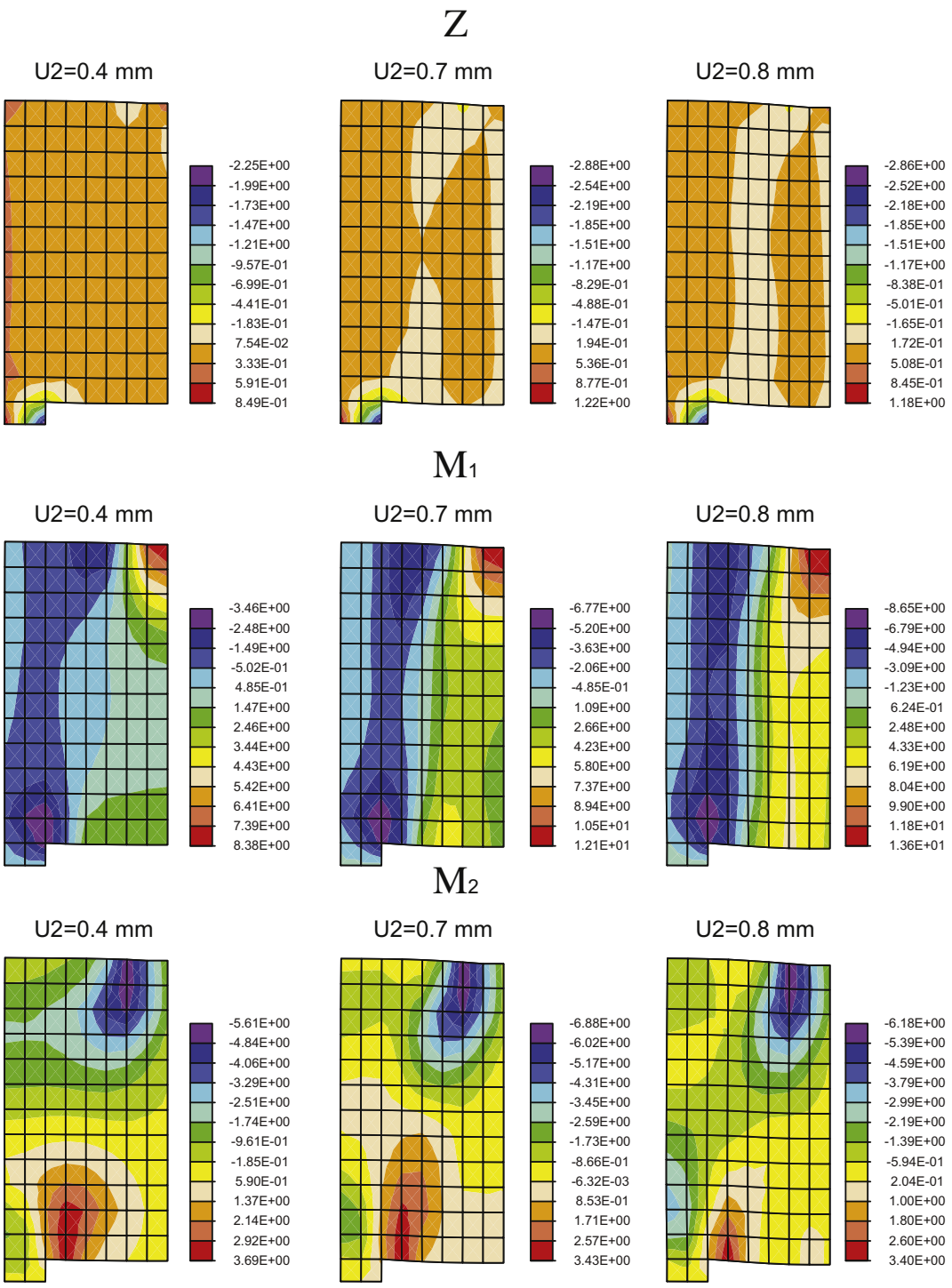

Fig. 12. Masonry panel under vertical load: macroscopic stresses Z (first row), M_1 (second row) and M_2 (third row) evaluated at different values of the applied vertical displacement.

the bottom side with two steel rollers and the vertical external load was applied through steel plates located on the top side of the panel as shown in Fig. 7. The geometrical parameters of bricks and mortar are the following: size of the brick $b = 56$ mm, $h = 15$ mm; thickness of the mortar joints $s = 2$ mm. Furthermore, the material mechanical parameters are:

	E (MPa)	v	$\varepsilon_{N,0}$	$\gamma_{NT,0}$	G_{cI} (MPa)	G_{cII} (MPa)	μ_i	μ_f	δ	σ_y (MPa)	α (MPa)
Brick	1850	0.15									
Mortar	233	0.15	0.0015	0.004	0.00096	0.0057	0.4	0.35	3.0	5	0

where E and v are Young's and Poisson moduli, respectively. Due to the symmetry of the problem, only one half of the panel is analyzed and two meshes with 74 (Fig. 7a) and 98 (Fig. 7b) FEs are adopted. A distributed vertical displacement is applied at the last three nodes of the top side. The steel rollers are discretized by means of 4-node quadrilateral FEs, assuming a linear elastic constitutive law with Young's modulus equal to 210,000 MPa and Poisson modulus 0.3. In Fig. 8 the global response curve of the panel is shown, i.e. the global vertical reaction computed at the restrained node of the bottom side versus the top applied displacement is depicted. The three different curves shown refer to the numerically obtained results (solid and dashed lines) and the experimental ones (line with diamond symbols). As it can be noted the numerical curves are in a good agreement with the experimental one. In order to obtain a macroscopic homogenized evaluation of the damage variable in the RVE, two average damage variables are computed, one corresponding to the damage distribution in the horizontal joints, the other to the damage in the vertical points. Then, in Fig. 9 the distributions of the damage variable are reported for the vertical head joints (left column) and the horizontal bed joints (right column), respectively, and at three values of the applied vertical displacement, $U_2 = 0.4$ mm, $U_2 = 0.7$ mm and $U_2 = 0.8$ mm, corresponding to the activation of the damage mechanisms, the reaching of the peak load value and the initiation of the softening phase. The initial linear elastic behavior is followed by a nonlinear hardening phase during which the damage starts first in the horizontal joints (at $U_2 = 0.3$ mm approximately) in the two regions located at the bottom, near the steel rollers, and at the top, near the ends of the steel plate, where the load is applied. Then, damage appears also in the vertical joints located near the bottom side mainly concentrated at the right corner, i.e. at the centre of the side where the flexural deformation state is more important. The global response curve reaches a peak load of 760 da N which matches very well the experimental value, at the applied displacement value of 0.7 mm. After that the global response curve shows a softening trend, during which the damage in both the horizontal and vertical joints spreads in a vertical band corresponding to the formation of the micro-fracture mechanisms typical of the experimental test. In Fig. 10 the distributions of the rigid rotation W and the Cosserat rotation component Φ is shown at the same values of the imposed vertical displacement. Although the distributions of the two rotations appear similar, the values of the Cosserat rotation in the panel differ from the ones of the rigid rotation, showing that the micropolar Cosserat model adopted at the macro-level allows to describe the rotational deformation of the RVE, which is relevant in this example and is on the other hand neglected by the standard Cauchy model. Lastly, in Figs. 11 and 12 the homogenized macroscopic stress components are reported. In particular, in Fig. 11 the Cauchy in-plane stresses Σ_1, Σ_2 and Σ_{12} are shown, while Fig. 12 contains the additional Cosserat stress components Z, M_1 and M_2. Note that the maximum values of the micro-couples appear near the end zones of the loaded and restrained areas, where also the rotations are relevant.

5.4. Pre-stressed shearing masonry wall

The masonry wall shown in Fig. 13 is analyzed. It was studied experimentally by Raijmakers and Vermeltfoort (1992). The dimensions of the wall are: width $B = 990$ mm, eight $H = 1000$ mm, thickness $T = 100$ mm. It is build up with 18 corses of clay bricks, the first and last of which being clamped in steel beams. The wall is subjected initially to a vertical compressive load uniformly applied at the top side equal to 0.30 MPa. During this phase the wall is completely restrained at the bottom side. Subsequently, also the vertical translation and the rotation of the top side is

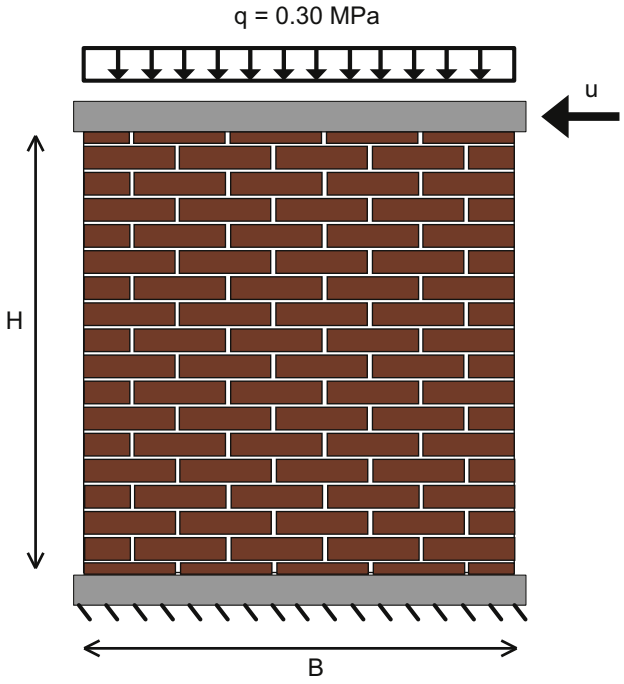

Fig. 13. Shearing masonry wall: geometry and boundary conditions.

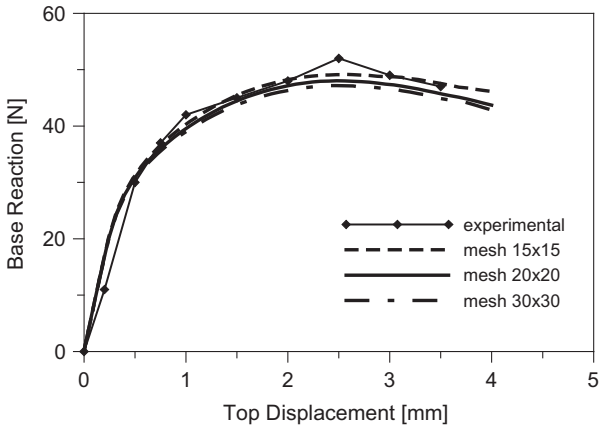

Fig. 14. Shearing masonry wall: global response curve.

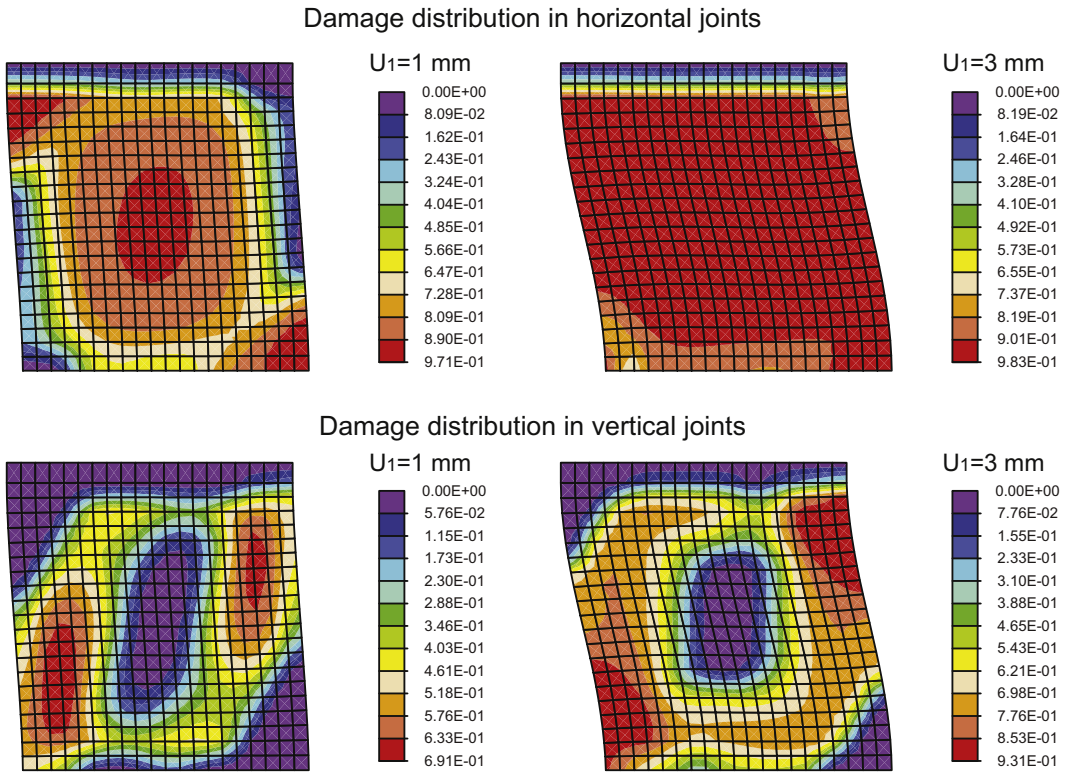

Fig. 15. Shearing masonry wall: damage distributions in horizontal (first line) and vertical joints (second line) evaluated at different values of the applied horizontal displacement.

restrained and a horizontal leftward displacement monotonically increasing until the value of 4 mm is applied to these nodes. The geometrical parameters of bricks and mortar are the following: size of the brick $b = 210$ mm, $h = 52$ mm; thickness of the mortar joints $s = 10$ mm. Furthermore, the material mechanical parameters are:

	E (MPa)	v	$\varepsilon_{N,0}$	$\gamma_{NT,0}$	G_{cI} (MPa)	G_{cII} (MPa)	μ_i	μ_f	δ	σ_y (MPa)	α (MPa)
Brick	16,700	0.15									
Mortar	798	0.11	0.0003	0.001	0.00179	0.0126	0.47	0.01	2.5	5	0

where E and v are Young's and Poisson moduli, respectively. Three different meshes are adopted with 15×15, 20×20 and 30×30 FEs, respectively. To model the top steel beam 4-node quadrilateral FEs are used, assuming a linear elastic constitutive law with Young's modulus equal to 167,000 MPa and Poisson modulus 0.15. In Fig. 14 the global response curve of the wall is reported. In particular, the global horizontal reaction computed at the bottom side versus the top applied displacement is depicted. Four different curves are shown referring to the numerically obtained results and the experimental ones (line with diamond symbols). It is evident that the numerical curves match very well the experimental one. Furthermore, the dash line curve referring to the 15×15 mesh is not a perfectly converged solution, while the solid and dash-dot line curves referring to the finer mesh are undistinguishable, so proving the capability of the Cosserat model adopted at the macro-level to lead to mesh-independent FE results. After the initial linear elastic behavior, the nonlinear mechanisms are activated and the global response curve reaches a peak load of around 48 N, a little lower than the experimentally calculated one, at the applied displacement value of 2.5 mm. Then, the global response curve shows a softening trend. In Fig. 15 the map of the macroscopic damage variable is reported for the horizontal bed joints (first line) and the vertical head joints (second line), respectively, and at two values of the top applied displacement, $U_1 = 1$ mm and $U_1 = 3$ mm. By observing the first line, it can be seen that damage starts in the bed joints located at the bottom right and top left of the wall, where it experiences the most severe flexural deformation state. After, damage spreads involving also the bed joints located near the center of the wall, where the shear mechanisms are predominant. As for the damage in the vertical joints, it is mainly concentrated into two vertical bands.

6. Conclusions

A multi-scale procedure has been proposed adopting a Cosserat model at the macro-level and the classical Cauchy continuum at the micro-scale. The use of the enriched micropolar formulation has resulted in two main advantages also demonstrated by the numerical applications. From a mechanical point of view Cosserat model has been able to describe typical micromechanical mechanisms not recovered by the Cauchy medium, like the rotation of the blocks as well as additional deformation components like as the rotational deformation and the two curvatures. In many practical applications on structural masonry panels, like the examples proposed in this paper, such deformation mechanisms can be relevant. Moreover, another important property of the Cosserat model has emerged due to the inner capability of regularizing the numerical

FE response in presence of strain-softening behavior, at least when the damaging mechanisms are of shearing type. This has been clearly showed in one of the numerical applications presented. It is worthwhile noting that the inner regularization properties of the Cosserat formulation have avoided the adoption of a numerical regularization technique and the related identification of the characteristic length, since it naturally arises from the adopted formulation with a clear mechanical meaning. In the spirit of the multi-scale modeling, coarse FE discretizations should be chosen in order to get the size of the FEs greater than the microstructural characteristic length. Nevertheless, considering the different FE meshes adopted in the numerical examples for reproducing experimental tests, it is important to underline that they have been selected to accurately model the boundary conditions, i.e. loads and restraints. The two experimental examples reproduced in this paper have been selected since the experimental data were available in literature (example presented in Section 5.4), or it concerned an in-house experimental test (example presented in Section 5.3).

At the micro-level a damage-plastic constitutive model has been introduced capable to describe the main relevant micromechanical inelastic mechanisms such as the damage, the friction plasticity and the crushing of the mortar joints, while the inelastic behavior of the blocks has not been considered. In particular, the formulation of the constitutive model proposed has been enriched with respect to the one adopted in previous papers by the same authors, considering here also the crushing plasticity mechanisms and a degrading exponential law for the friction parameter, consistent with the experimental results. The presented multi-scale formulation based on the TFA homogenization technique has resulted very effective from a computational point of view, since it has allowed to reduce considerably the computational burden with respect to the standard homogenization procedures, avoiding to solve nested micromechanical FE problems at each Gauss point of the macro-level discretization. At the same time it has been able to analyze interesting structural cases describing also the details of the micromechanical mechanisms and giving results in a great agreement with the experimental ones.

References

Addessi, D., Sacco, E., Paolone, A., 2010. Cosserat model for periodic masonry deduced by nonlinear homogenization. European Journal of Mechanics – A/Solids 29, 724–737.

Alfano, G., Sacco, E., 2006. Combining interface damage and friction in a cohesive-zone model. International Journal for Numerical Methods in Engineering 68 (5), 542–582.

Anthoine, A., 1995. Derivation of the in-plane elastic characteristics of masonry through homogenization theory. International Journal of Solids and Structures 32 (2), 137–163.

Bacigalupo, A., Gambarotta, L., 2011. Second-order computational homogenization of heterogeneous materials with periodic microstructure. ZAMM: Journal of Applied Mathematics and Mechanics 90 (10-11), 796811.

Bazant, Z., Planas, J., 1998. Fracture and Size Effects in Concrete and Other Quasibrittle Materials. CRC Press LLC.

Brasile, S., Casciaro, R., Formica, G., 2007a. Multilevel approach for brick masonry walls. Part i: A numerical strategy for the nonlinear analysis. Computer Methods in Applied Mechanics and Engineering 196, 4934–4951.

Brasile, S., Casciaro, R., Formica, G., 2007b. Multilevel approach for brick masonry walls. Part ii: On the use of equivalent continua. Computer Methods in Applied Mechanics and Engineering 196, 4801–4810.

Casolo, S., 2006. Macroscopic modelling of structured materials: relationship between orthotropic Cosserat continuum and rigid elements. International Journal of Solids and Structures 43 (3–4), 475–496.

Cavalagli, N., Cluni, F., Gusella, V., 2011. Strength domain of non-periodic masonry by homogenization in generalized plane state. European Journal of Mechanics – A/Solids 30, 113–126.

Cecchi, A., Sab, K., 2009. Discrete and continuous models for in plane loaded random elastic brickwork. European Journal of Mechanics – A/Solids 28, 610–625.

De Bellis, M., Addessi, D., 2011. A Cosserat based multi-scale model for masonry structures. International Journal for Computational Engineering 9 (5), 543–563.

Dvorak, G., 1992. Transformation field analysis of inelastic composite materials. Proceedings of the Royal Society of London A 437, 311–327.

Fish, J., Shek, K., 2000. Multiscale analysis of composite materials and structures. Composites Science and Technology 60, 2547–2556.

Forest, S., Sab, K., 1998. Cosserat overall modelling of heterogeneous materials. Mechanics Research Communications in Numerical Methods in Engineering 4, 449–454.

Gambarotta, L., Lagomarsino, S., 1997a. Damage models for the seismic response of brick masonry shear walls. Part i: The mortar joint model and its application. Earthquake Engineering and Structural Dynamics 26, 423–439.

Gambarotta, L., Lagomarsino, S., 1997b. Damage models for the seismic response of brick masonry shear walls part ii: the continuum model and its application. Earthquake Engineering and Structural Dynamics 26, 441–462.

Grande, E., Milani, G., Sacco, E., 2008. Modelling and analysis of frp-strengthened masonry panels. Engineering Structures 30, 18421860.

Kouznetsova, V.G., Geers, M.G.D., Brekelmans, W.A.M., 2002. Multi-scale constitutive modelling of heterogeneous materials with a gradient-enhanced computational homogenization scheme. International Journal for Numerical Methods in Engineering 54, 1235–1260.

Linder, C., Armero, F., 2007. Finite elements with embedded strong discontinuities for the modeling of failure in solids. International Journal for Numerical Methods in Engineering 72 (12), 1391–1433.

Luciano, R., Sacco, E., 1998. Variational methods for the homogenization of periodic heterogeneous media. European Journal of Mechanics – A/Solids 17 (4), 599–617.

Masiani, R., Rizzi, R., Trovalusci, P., 1995. Masonry as structured continuum. Meccanica 30 (6), 673–683.

Masiani, R., Trovalusci, P., 1996. Cauchy and Cosserat materials as continuum models of brick masonry. Meccanica 31 (4), 421432.

Massart, T.J., Peerlings, R.H.J., Geers, M.G.D., 2007. An enhanced multi-scale approach for masonry wall computations with localization of damage. International Journal for Numerical Methods in Engineering 69 (5), 1022–1059.

Massart, T.J., Peerlings, R.H.J., Geers, M.G.D., Gottcheiner, S., 2005. Mesoscopic modeling of failure in brick masonry accounting for three-dimensional effects. Engineering Fracture Mechanics 72 (8), 1238–1253.

Mercatoris, B., Massart, T., 2011. A coupled two-scale computational scheme for the failure of periodic quasi-brittle thin planar shells and its application to masonry. International Journal for Numerical Methods in Engineering 85, 1177–1206.

Pegon, P., Anthoine, A., 1997. Numerical strategies for solving continuum damage problems with softening: application to the homogenization of masonry. Computers and Structures 64, 623–642.

Ragueneau, F., La Borderie, C., Mazars, J., 2000. Damage model for concrete-like materials coupling cracking and friction, contribution towards structural damping: first uniaxial applications. Mechanics of Cohesive-Frictional Materials 5 (8), 607–625.

Raijmakers, T.M.J., Vermeltfoort, A.T., 1992. Deformation controlled tests in masonry shear walls. Report B-92-1156. TNO-Bouw, Delft, The Netherlands.

Sab, K., Pradel, F., 2009. Homogenisation of periodic Cosserat media. International Journal of Computer Applications in Technology 34 (1), 60–71.

Sacco, E., 2009. A nonlinear homogenization procedure for periodic masonry. European Journal of Mechanics – A/Solids 28 (2), 209–222.

Salerno, G., de Felice, G., 2009. Continuum modeling of periodic brickwork. International Journal of Solids and Structures 46 (5), 1251–1267.

Simo, J., Hughes, T.J.R., 1998. Computational Inelasticity. Springer, New York.

Suquet, P., 1987. Elements of homogenization for inelastic solid mechanics. In: Homogenization Techniques for Composite Media. Springer-Verlag, Berlin.

Taylor, R., 2011. FEAP – a finite element analysis program, Version 8.3. Department of Civil and Environmental Engineering, University of California at Berkeley, California.

Terada, K., Hori, M., Kyoya, T., Kikuchi, N., 2000. Simulation of the multi-scale convergence in computational homogenization approach. International Journal of Solids and Structures 37, 2285–2311.

Trovalusci, P., Masiani, R., 1999. Material symmetries of micropolar continua equivalent to lattices. International Journal of Solids and Structures 36 (14), 2091–2108.

van der Sluis, O., Schreurs, P.J.G., Brekelmans, W.A.M., Meijer, H.E.H., 2000. Overall behaviour of heterogeneous elastoviscoplastic materials: effect of microstructural modelling. Mechanics of Materials 32, 449–462.

Wei, X., Hao, H., 2009. Numerical derivation of homogenized dynamic masonry material properties with strain rate effects. International Journal of Impact Engineering 36, 522–536.

Zucchini, A., Lourenco, P., 2009. A micromechanical homogenisation model for masonry: Application to shear walls. International Journal of Solids and Structures 46 (3–4), 871–886.